



HAL
open science

Elemental geochemistry and Nd isotope constraints on the provenance of the basal siliciclastic succession of the middle Paleoproterozoic Francevillian Group, Gabon

Olabode Bankole, Abderrazak El Albani, Alain Meunier, Marc Poujol, Andrey Bekker

► To cite this version:

Olabode Bankole, Abderrazak El Albani, Alain Meunier, Marc Poujol, Andrey Bekker. Elemental geochemistry and Nd isotope constraints on the provenance of the basal siliciclastic succession of the middle Paleoproterozoic Francevillian Group, Gabon. *Precambrian Research*, 2020, 348, pp.105874. 10.1016/j.precamres.2020.105874 . insu-02903479

HAL Id: insu-02903479

<https://insu.hal.science/insu-02903479>

Submitted on 21 Jul 2020

HAL is a multi-disciplinary open access archive for the deposit and dissemination of scientific research documents, whether they are published or not. The documents may come from teaching and research institutions in France or abroad, or from public or private research centers.

L'archive ouverte pluridisciplinaire **HAL**, est destinée au dépôt et à la diffusion de documents scientifiques de niveau recherche, publiés ou non, émanant des établissements d'enseignement et de recherche français ou étrangers, des laboratoires publics ou privés.

Journal Pre-proofs

Elemental geochemistry and Nd isotope constraints on the provenance of the basal siliciclastic succession of the middle Paleoproterozoic Francevillian Group, Gabon

Olabode M. Bankole, Abderrazak El Albani, Alain Meunier, Marc Poujol, Andrey Bekker

PII: S0301-9268(19)30560-1
DOI: <https://doi.org/10.1016/j.precamres.2020.105874>
Reference: PRECAM 105874

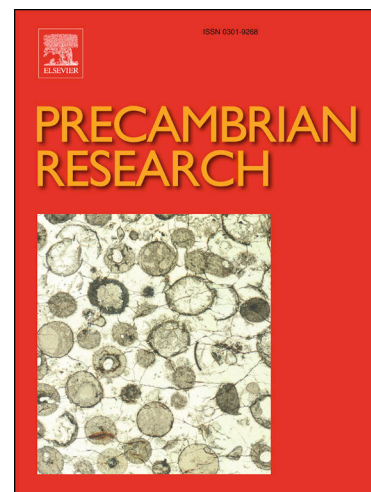
To appear in: *Precambrian Research*

Received Date: 1 October 2019
Revised Date: 8 July 2020
Accepted Date: 15 July 2020

Please cite this article as: O.M. Bankole, A. El Albani, A. Meunier, M. Poujol, A. Bekker, Elemental geochemistry and Nd isotope constraints on the provenance of the basal siliciclastic succession of the middle Paleoproterozoic Francevillian Group, Gabon, *Precambrian Research* (2020), doi: <https://doi.org/10.1016/j.precamres.2020.105874>

This is a PDF file of an article that has undergone enhancements after acceptance, such as the addition of a cover page and metadata, and formatting for readability, but it is not yet the definitive version of record. This version will undergo additional copyediting, typesetting and review before it is published in its final form, but we are providing this version to give early visibility of the article. Please note that, during the production process, errors may be discovered which could affect the content, and all legal disclaimers that apply to the journal pertain.

© 2020 Published by Elsevier B.V.



1 **Elemental geochemistry and Nd isotope constraints on the provenance of**
2 **the basal siliciclastic succession of the middle Paleoproterozoic**
3 **Francevillian Group, Gabon**

4 Olabode M. Bankole^{1*}, Abderrazak El Albani¹, Alain Meunier¹, Marc Poujol², Andrey
5 Bekker^{3,4}

6
7 ¹Geosciences-IC2MP, UMR CNRS 7285, Université de Poitiers, 86073 Poitiers, France

8 ²Univ Rennes, CNRS, Géosciences Rennes - UMR 6118, F-35000 Rennes, France

9 ³Department of Earth and Planetary Sciences, University of California, Riverside, California
10 92521, USA

11 ⁴ Department of Geology, University of Johannesburg, Auckland Park 2006, South Africa

12
13 *Corresponding author: olabode.bankole@univ-poitiers.fr

14
15 **Abstract**

16 Whole-rock elemental geochemistry and Nd isotope composition of siliciclastic rocks from
17 the basal part of the unmetamorphosed middle Paleoproterozoic Francevillian Group, Gabon
18 (FA Formation and FB₁ Member) were examined to provide insights into their provenance
19 and its crustal evolution. Chemical weathering index diagrams suggest moderate degree of
20 weathering in the provenance and secondary K-addition during illitization. Trace element
21 geochemical proxies including the REEs provide evidence for sediment derivation from
22 felsic-dominated upper continental crust (UCC) similar to Archean trondhjemite-tonalite-
23 granodiorite (TTG) with minor contribution of mafic components. The low ¹⁴³Nd/¹⁴⁴Nd and
24 negative εNd values (-10.83 to -5.76) provide further evidence for old and evolved upper
25 continental crust components in detrital sources. The depleted mantle model ages for the

26 provenance protolith (2.73-3.05 Ga) are consistent with sediments sourced from the
27 Mesoarchean granitoids of East Gabonian block exposed in the northern and southern parts of
28 Gabon. We infer that the evolved, Mesoarchean felsic TTG-like granitoids were the main
29 source for the sediments of the basal Francevillian Group, while minor mafic inputs from the
30 contemporaneous greenstone belt with the Belinga Group cannot be completely discounted.
31 The predominantly old crustal sources for the sediments suggest crustal addition and
32 recycling of differentiated granitoid plutons instead of formation of juvenile crust during
33 deposition in the Francevillian basin.

34 **Keywords:** Elemental geochemistry, Nd isotope, provenance, Mesoarchean, Francevillian
35 Group, Gabon

36

37 1. Introduction

38 The middle Paleoproterozoic Francevillian basin developed in southeastern Gabon and
39 hosting the Francevillian Group, is one of the world's most studied and least deformed middle
40 Paleoproterozoic sedimentary successions. Compared to sedimentary successions of similar
41 age that have been highly deformed and altered, the Francevillian basin sediments were not
42 metamorphosed and have only been affected by diagenetic and/or low-temperature
43 hydrothermal processes (Bros et al., 1992; Gauthier-Lafaye and Weber, 1989, 2003; Mathieu
44 et al., 2001; Bankole et al., 2015, 2016, 2018). Thus, the basin has been extensively studied
45 and is well known for the oldest high-grade, redox-controlled, and sandstone-hosted uranium
46 ore mineralization (Gauthier-Lafaye and Weber, 1989, 2003; Bankole et al., 2016), natural
47 fossil nuclear-fission reactors (Gauthier-Lafaye and Weber, 1989), oldest multicellular
48 microfossils (El Albani et al., 2019, 2014), and hosts the third largest known manganese-ore
49 reserve in the world (Gauthier-Lafaye and Weber, 2003; Gauthier-Lafaye, 2006).

50 Although a number of studies have been carried out on the Francevillian Group, little
51 is known about the geochemical characteristics of the sediments and their provenance has not
52 previously been studied in much details. The geochemical composition of siliciclastic rocks is
53 useful in providing information about their provenance, including its age and crustal
54 evolution, surface Earth processes, and tectonic setting of sedimentary basins (McLennan et
55 al., 2003). Thiéblemont et al. (2009) and Weber et al. (2016) used geochemical datasets for
56 the Okondja sub-basin to suggest a change from rift-related deposition of the FA Formation to
57 subduction-related tectonic setting with accompanying alkaline, mafic to ultramafic
58 magmatism at the time when the FB Formation was deposited. However, Bankole et al.
59 (2018) inferred from geochemical data that the interlayered thin K-bentonite beds in the FB_{2b}
60 unit in the Franceville sub-basin were derived from calc-alkaline intermediate to felsic
61 magmatism, which was related to a continental arc in a subduction setting developed during
62 plate convergence. Recently, Ossa Ossa et al. (2020) utilized detrital zircon geochronology to
63 suggest that the uranium-bearing sandstones and conglomerates of the FA and FB formations
64 in the Francevillian basin were mainly sourced from the Mesoarchean granitoids of the East
65 Gabonian block of the northwestern Congo craton.

66 This study presents new whole-rock elemental and Nd isotope data for the two basal
67 sedimentary units of the Francevillian Group, FA and FB formations, in the Francevillian
68 basin. We screened first for post-depositional overprints and elemental mobility to establish
69 preservation of primary geochemical signals before constraining the intensity of chemical
70 weathering, provenance, and tectonic setting for the sedimentary rocks of the FA and lower
71 FB (FB₁ Member) formations as well as crustal evolution of their provenance.

72

73

74 2. Geological Background

75 The middle Paleoproterozoic Francevillian Group is an extensive sequence of
76 unmetamorphosed siliciclastic and volcanoclastic strata that unconformably overlie the
77 Archean basement rocks of the northwestern part of the Archean Congo craton in central to
78 southeastern Gabon (Fig. 1). The basin is bounded by the Mesoarchean (3185-2805 Ma) and
79 Neoproterozoic (2802-2500 Ma) granitoids of the East Gabonian block on the north (North
80 Gabon massif) and south (Chaillu massif) and by the Neoproterozoic to early Paleoproterozoic
81 (ca. 2515-2435 Ma) migmatites and Paleoproterozoic (ca. 2200-2120 Ma) supracrustal rocks
82 of the Ogooué orogenic belt (West Gabonian block) to the west (Fig. 1; Caen-Vachette et al.,
83 1988; Feybesse et al., 1998; Ledru et al., 1989; Thiéblemont et al., 2009). The Mesoarchean
84 rocks of the East Gabonian block are composed of calc-alkaline and TTG (tonalite-
85 trondhjemite-granodiorite) gneisses and granitoids with minor occurrences of ca. 2820 Ma
86 charnockites and ca. 2920-2750 Ma greenstone belts. The greenstone belts are composed of
87 the stratigraphic unit called Belinga Group, which includes mafic to ultramafic volcanic
88 rocks, BIFs (banded iron formations), conglomerates, and micaschists. The Neoproterozoic
89 basement rocks of the East and West Gabonian blocks consist of metamorphosed (gneisses
90 and migmatites) and unmetamorphosed (diorites, granites, and syenites) rocks. The Ogooué
91 orogenic belt of the West Gabonian block is bounded by the Ikoy-Ikobé fault to the west and
92 the Ogooué thrust (Lopé High) to the east and was formed during the 2.2-2.0 Ga Eburnean
93 orogeny, which involved collision of the Congo and São Francisco cratons, and several
94 Paleoproterozoic orogenic events in the western and central parts of Africa (Ledru et al.,
95 1989; Feybesse et al., 1998; Weber et al., 2016). It is a fold-and-thrust belt composed of
96 greenschist to amphibolite facies metasediments and metavolcanic rocks with a peak
97 metamorphism at 2120 ± 38 Ma (Feybesse et al., 1998; Weber et al., 2016). Time-equivalent
98 successions on the São Francisco craton include the Monteiro sequence of the Rio Itapicuru

99 greenstone belt on the western Serrinha block in eastern Bahia, Brazil (Grisolia and Oliveira,
100 2012; Oliveira et al., 2010), and the Cercadinho-Sabar formations of the Minas Supergroup
101 (Quadriltero Ferrfero mining district, Minas Gerais, Brazil) (Bekker et al., 2003;
102 Maheshwari et al., 2010; Reis et al., 2002). These two successions were deposited in foreland
103 basins during the ca. 2.08-2.04 Ga collision of the Congo and So Francisco cratons,
104 potentially in the aftermath of the assembly of the West and East Gabonian blocks.
105 Geochemical signatures for these successions are consistent with sediment supply from
106 continental arcs (e.g., Grisolia and Oliveira, 2012; Reis et al., 2002). Speculatively,
107 development of the Francevillian basin could therefore represent a distal response to collision
108 of the Congo and So Francisco cratons.

109 The Francevillian basin, hosting sediments of the Francevillian Group, is bounded by
110 the Ogoou thrust to the west and overlain by the horizontally laying formations of the
111 Mesozoic Congo basin to the east. The Francevillian Group consists of volcano-sedimentary
112 strata that are exposed in Okondja, Lastourville, Franceville, and Boou sub-basins (Fig. 1;
113 Bonhomme et al., 1982; Gauthier-Lafaye and Weber, 1989; Bros et al., 1992; Gauthier-
114 Lafaye, 2006; Prat et al., 2011). Although the tectonic setting and development of the
115 Francevillian basin remain debated (Feybesse et al., 1998; Thiblemont et al., 2014; Weber et
116 al., 2016), its geodynamic evolution has been tied to the supercontinent tectonic cycle that
117 started with the break-up of the Archean supercraton Superia and led during the Eburnean
118 orogeny to the formation of the West Central African Belt (WCAB), which subsequently
119 became the core of the Nuna supercontinent. The Francevillian Group has been divided into
120 five lithostratigraphic formations, FA to FE from the base to top, in the Franceville and
121 Okondja sub-basins (Fig. 2; Weber, 1968).

122 The lower part of the FA Formation, consisting mainly of coarse-grained sandstones
123 and conglomerates with minor intercalations of fine-grained sandstones and mudstones, was

124 unconformably deposited on the Archean crystalline basement in a braided fluvial
125 environment (Haubensack, 1981; Gauthier-Lafaye and Weber, 1989; Bankole et al., 2015).
126 The upper part of the FA Formation is dominated by fine-grained sandstones and mudstones
127 with interbedded coarse-grained sandstones, and has been interpreted to indicate fluvio-deltaic
128 sedimentation. All the uranium ore deposits are hosted in the upper FA Formation sandstones.
129 The overlying FB Formation is a heterogeneous succession of intertidal and subtidal
130 mudstones and black shales with interbedded fine- to coarse-grained sandstones, breccias, and
131 conglomerates (Azzibrouck-Azziley, 1986; Canfield et al., 2013; El Albani et al., 2010;
132 Gauthier-Lafaye and Weber, 1989, 2003; Ossa Ossa et al., 2013, 2018; Pambo, 2004; Pr at et
133 al., 2011; Reynaud et al., 2017; Weber, 1968). The FB Formation has been divided into FB₁
134 and FB₂ members based on lithological differences and sedimentary structures (Fig. 2b). The
135 transition from FA to FB Formation occurred during marine transgression induced by tectonic
136 subsidence in the foreland basin in front of the forebulge (Ossa Ossa et al., 2020) and
137 associated with the appearance of polygenetic breccias and olistolithes on the present-day
138 southwestern margin of the Franceville and Okondja sub-basins (Gauthier-Lafaye and Weber,
139 2003, 1989). The FC Formation is composed of shallow-marine to supratidal (sabkha)
140 deposits of massive dolostone and stromatolitic chert with thin beds of black shale (Gauthier-
141 Lafaye and Weber, 2003; Pr at et al., 2011; Ossa Ossa et al., 2018). The FD Formation
142 consists of rhyolitic tuffs and epiclastic sandstones interbedded with marine black shales at
143 the top, while the uppermost FE Formation is dominated by cross-bedded, coarse-grained to
144 conglomeratic arkosic sandstones (Gauthier-Lafaye and Weber, 2003; Thi blemont et al.,
145 2014).

146 The age and the duration of deposition of the Francevillian Group have not been fully
147 resolved, but several attempts have been made to constrain the depositional age of the
148 sedimentary strata. Sm-Nd isotope systematics was used to constrain the age of early

149 diagenesis of the FB_{1b} unit in the Franceville sub-basin with <0.4 μm and <0.2 μm clay
150 fractions at 2099 ± 115 Ma and 2036 ± 79 Ma, respectively (Bros et al., 1992). The age of late
151 diagenesis of the FB_{1c} unit was constrained with <1.5 μm and <2.0 μm authigenic illites that
152 produced an apparent Rb-Sr isochron date of 1870 ± 50 Ma (Bonhomme et al., 1982). Horie
153 et al. (2005) obtained a precise U-Pb SHRIMP zircon date of 2083 ± 6 Ma for the ignimbrite
154 tuff in the FD Formation for which analytical data was not yet published. Bonhomme et al.
155 (1982) reported a Rb-Sr whole-rock age of 2143 ± 143 Ma for coarse-grained syenites of the
156 N’Goutou alkaline complex that intrudes the FA and FB formations in the Okondja basin
157 (Fig. 1). Recently, Sawaki et al. (2017) published new highly discordant MC-ICP-MS ^{207}Pb -
158 ^{206}Pb zircon age of 2191 ± 12 Ma for the N’Goutou Complex, which, if correct, would place
159 the depositional age of the Francevillian Group to the beginning of the Lomagundi carbon
160 isotope excursion. The FB and FC formations are considered to record the end of the 2.22 to
161 2.06 Ga Lomagundi carbon isotope excursion based on $\delta^{13}\text{C}_{\text{carb}}$ and $\delta^{13}\text{C}_{\text{org}}$ trends, and to be
162 correlative with the Zaonega Formation in the Onega basin of Karelia, Russia (Kump et al.,
163 2011), which is also imprecisely dated (Martin et al., 2015; Ovchinnikova et al., 2007).
164 Elsewhere in Fennoscandia, the end of the Lomagundi carbon isotope excursion is placed
165 between 2.11 and 2.06 Ga (Karhu and Holland, 1996; Martin et al., 2013). Combined, these
166 age constraints place the age of deposition for the Francevillian Group close to 2.11 to 2.06
167 Ga, and currently provides the best estimate for the depositional age of the Francevillian
168 Group (Canfield et al., 2013).

169 Detailed discussion of lithostratigraphy, depositional facies, petrography, diagenesis,
170 and mineral chemistry of the basal part of the FA Formation and FB₁ Member in the
171 Franceville sub-basin (this study area) are given in Bankole (2015) and Bankole et al. (2015,
172 2016). Additional information on the stratigraphy and depositional environment of the

173 Francevillian Group are provided Haubensack (1981), Gauthier-Lafaye (1986), Gauthier-
174 Lafaye and Weber (1989, 2003) and Reynaud et al., (2017).

175

176

177 3. Samples and Analytical Techniques

178 Surface outcrops of the FA Formation and FB₁ Member are strongly weathered in the
179 Francevillian basin; therefore, only fresh drill core samples were used for sampling. Samples
180 for this study were collected from eight drill cores from the proximal to distal parts of the
181 Franceville sub-basin (Figs. 2a and 3). Most of the drill cores intersected the transition zone
182 between the upper FA and lower FB formations, except for the BA 2 and GR 15 drill cores
183 where only the FA Formation was encountered. The FA and FB formation sediments as well
184 as their boundary were defined based on distinct lithologies and drill core logs. All the studied
185 samples were carefully cut from drill cores to minimize effect of recent weathering and
186 alteration. We selected 54 samples, including 41 shales and siltstones and 13 sandstones,
187 representing all the major lithological units across the FA Formation and FB₁ Member for
188 geochemical analysis (Fig. 3). All the sandstones are from the FA Formation. The analyzed
189 samples are broadly classified in this study into two main groups: mudstones (shales and
190 siltstones) and sandstones (fine- to coarse-grained sandstones).

191 All the selected 54 samples were powdered in agate mortar, and analyzed for whole-
192 rock major and trace element compositions at the *Service d'Analyse des Roches et des*
193 *Mineraux* (SARM; CRPG-CNRS), Nancy, France. The whole-rock powder of ~100 mg of
194 each sample was fused with lithium metaborate (LiBO₂) and dissolved in nitric acid for
195 elemental analysis. Major and trace element data were obtained using inductively coupled
196 plasma atomic emission spectrometry (ICP-AES) and inductively coupled plasma mass

197 spectrometry (ICP-MS), respectively, following the techniques described in Carignan et al.
198 (2001).

199 Whole-rock Sm-Nd isotope analyses of 30 selected samples were carried out on the 7
200 collector Finnigan MAT-262 mass spectrometer at the GeOHeLis analytical facility
201 (Géosciences Rennes/OSUR, University of Rennes, France). Samples were spiked with a
202 ^{149}Sm - ^{150}Nd mixed solution and dissolved in a 2:1 acid mixture of 23 mol/L HF with 15
203 mol/L HNO_3 . They were then dried and taken up with 6 mol/L HCl. In each analytical
204 session, the unknowns were analyzed together with the Ames Nd-1 Nd standard, which during
205 the course of this study yielded average $^{143}\text{Nd}/^{144}\text{Nd}$ values of 0.511938 ± 5 (session 1),
206 0.511939 ± 5 (session 2), and 0.511928 ± 5 (session 3). All data for the unknowns have been
207 adjusted to the long-term $^{143}\text{Nd}/^{144}\text{Nd}$ value of 0.511963 for Ames Nd-1. Instrumental mass
208 fractionation was monitored and corrected using the $^{146}\text{Nd}/^{144}\text{Nd}$ value of 0.7219. Procedural
209 blank analyses yielded 50 pg for Nd and the blank is therefore considered to be negligible.
210 The initial Nd-isotope composition ($\epsilon_{\text{Nd}(t)} = [((^{143}\text{Nd}/^{144}\text{Nd}_{\text{sample}}/^{143}\text{Nd}/^{144}\text{Nd}_{\text{CHUR}(t)} - 1) * 10^{-4})$),
211 depleted mantle model ages ($T_{\text{DM}} = (1/\lambda) * \ln[(^{143}\text{Nd}/^{144}\text{Nd}_{\text{sample}} -$
212 $^{143}\text{Nd}/^{144}\text{Nd}_{\text{DM}(0)}) / ((^{147}\text{Nd}/^{144}\text{Nd}_{\text{sample}} - ^{147}\text{Nd}/^{144}\text{Nd}_{\text{DM}(0)} + 1) * 10^{-9})]$), and fractional deviation of
213 $^{147}\text{Sm}/^{144}\text{Nd}$ from that of chondritic meteorites ($f^{\text{Sm}/\text{Nd}} = (^{147}\text{Sm}/^{144}\text{Nd})_{\text{sample}} / (^{147}\text{Sm}/^{144}\text{Nd})_{\text{CHUR}}$
214 $- 1$); McLennan et al., 1993) were calculated assuming present-day $^{143}\text{Nd}/^{144}\text{Nd}_{\text{CHUR}(0)} =$
215 0.512636 (CHUR: Chondritic Uniform Reservoir), $^{147}\text{Nd}/^{144}\text{Nd}_{\text{CHUR}(0)} = 0.1967$,
216 $^{143}\text{Nd}/^{144}\text{Nd}_{\text{DM}(0)} = 0.51235$, and $^{147}\text{Nd}/^{144}\text{Nd}_{\text{DM}(0)} = 0.217$, and decay constant, $\lambda = 6.54 \times 10^{-12}$
217 y^{-1} (DePaolo and Wasserburg, 1976). The initial $^{143}\text{Nd}/^{144}\text{Nd}$, $\epsilon_{\text{Nd}(t)}$ values, and T_{DM} ages for
218 the basal FA and FB formations sediments were calculated at depositional age of $t = 2.1$ Ga.

219

220

221 4. Results

222 4.1. Major element geochemistry

223 The major element data for the studied samples are presented in [Table A1 \(see](#)
224 [Appendix\)](#). The FA Formation sandstones falls within the arkose, sub-arkose, litharenite, and
225 quartz arenite compositional fields, whereas mudstones from FA Formation and FB₁ Member
226 fall within the shale and wacke fields in the Herron's (1988) geochemical classification
227 diagram for sedimentary rocks ([Fig. 4](#)). The sandstones generally have higher SiO₂/Al₂O₃
228 ratios and are therefore quartz-rich compared to the mudstone samples, which are clay-rich
229 ([Fig. 4](#)). Higher Fe₂O₃/K₂O ratios for the FB₁ Member mudstones compared to the FA
230 Formation mudstones and sandstones are related to the abundant Fe-rich dolomite and pyrite,
231 and the absence of K-feldspar in the FB Formation (Ngombi-Pemba et al., 2014; Bankole et
232 al., 2015, 2018). The K₂O/Al₂O₃ ratios are significantly lower for the FB₁ Member mudstones
233 (average = 15) compared to the FA Formation mudstones (average = 30) and FA sandstones
234 (average = 34), consistent with absence of K-feldspar in the FB Formation ([Table A1](#)).

235 Compared to the Late Archean Upper Continental Crust (LAUCC; Condie, 1993), the
236 analyzed samples, especially the FA Formation sandstones, are depleted in most of the major
237 elements ([Fig. A1; see Appendix](#)). All the FA Formation mudstones and few of the sandstone
238 samples are enriched in K₂O, whereas only few samples are enriched in Al₂O₃ and Fe₂O₃
239 relative to the FB₁ Member mudstones ([Fig. A1b](#)). The anomalously high MnO content in 2
240 FB₁ Member mudstones ([Fig. A1a](#)) is due to their stratigraphic proximity to the overlying Mn
241 protore hosted in this unit (Gauthier-Lafaye and Weber, 2003). The greatest elemental
242 variability is shown by the FA sandstones ([Fig. A1c](#)) and the slight enrichment in SiO₂
243 relative to the LAUCC reflects higher abundance of quartz in these samples. Enrichments in
244 Fe₂O₃, MnO, CaO, and MgO in some samples could be attributed to their high carbonate
245 content indicated by their large LOI values ([Table A1, see Appendix](#)).

246

247 4.2 Trace and rare earth element geochemistry

248 The trace and REE data are presented in [Tables A2 and A3 \(see Appendix\)](#). Although
249 the absolute concentrations of the trace elements are variable in the mudstone and sandstone
250 samples, their LAUCC-normalized patterns are rather similar ([Fig. 5](#)). The large-ion lithophile
251 elements (LILE) such as Rb, Ba, and U are moderately enriched in most of the FB₁ Member
252 and FA Formation mudstones ([Figs. 5a and b](#)), but significantly depleted in the FA Formation
253 sandstones ([Fig. 5c](#)). All of the samples are similarly depleted in Sr and Ca, which is likely
254 controlled by substitution of Sr for Ca in plagioclase. Concentrations of high-field strength
255 elements (HFSE) such as Zr, Hf, Y, Th, Ta, and Nb vary considerably regardless of the grain
256 size of the hosting lithology. Excluding few samples, the samples are depleted in Y, Nb, and
257 Ta, whereas Zr and Hf are relatively enriched in some of the FA Formation samples ([Figs. 5a-](#)
258 [c](#)) due to preferential enrichment in zircon during transport. All the transition trace elements
259 (TTE: Co, Cr, Sc, Ni, and V) are depleted in the FA Formation sandstones, but display
260 variable enrichments and depletions in the FA Formation and FB₁ Member mudstones.

261 While the REE have variable abundances, the chondrite-normalized REE patterns of
262 all the samples are remarkably similar among themselves and to the LAUCC ([Figs. 6a-c](#)). The
263 total REE abundances (Σ REE) are higher in the mudstones than in most of the sandstones
264 ([Table A3](#)), likely related to grain size and quartz dilution. The samples show significant
265 light-REE (LREE) enrichment (La_N/Yb_N), flat to slightly depleted heavy-REE (HREE),
266 negative to negligible Eu anomalies, and insignificant Ce anomalies. Very few samples have
267 La_N/Yb_N values smaller than the average chondrite value of 12.91 (McDonough and Sun,
268 1995). The FA Formation sandstones have variable and more pronounced negative Eu
269 anomalies ($Eu/Eu^* = 0.30-0.99$; average = 0.68) and generally higher La_N/Yb_N (7.20-92.63)
270 values than the FA Formation mudstones ($Eu/Eu^* = 0.69-0.95$; average = 0.81; $La_N/Yb_N =$

271 12.18-54.27) and FB₁ Member mudstones ($\text{Eu}/\text{Eu}^* = 0.72\text{-}0.95$; average = 0.85; $\text{La}_\text{N}/\text{Yb}_\text{N} =$
272 6.76-44.8).

273

274 4.3 Sm-Nd isotope geochemistry

275 The whole-rock Sm-Nd isotope data of the sandstones and mudstones is remarkably
276 similar and thus does not show any significant fractionation with respect to grain size (Table
277 1). The initial $^{143}\text{Nd}/^{144}\text{Nd}$ ratios for all the samples range from 0.5094 to 0.5096 and
278 $^{147}\text{Sm}/^{144}\text{Nd}$ ratios from 0.078 to 0.111, except for two outliers with considerably higher
279 values of 0.165 (BA 11_13.9) and 0.192 (GR_243.1) (Table 1; Figure A2). With the
280 exception of the two outlier samples, all the samples have overlapping negative $\epsilon_{\text{Nd}}(t)$ values
281 from -10.83 to -5.76, T_{DM} ages of 2.73 to 3.05 Ga, and $f^{\text{Sm}/\text{Nd}}$ from -0.60 to -0.43 (Table 1).
282 However, the two outliers with high $^{147}\text{Sm}/^{144}\text{Nd}$ ratios have unrealistically large T_{DM} dates of
283 5.72 and 6.03 Ga and $f^{\text{Sm}/\text{Nd}}$ of -0.16 and -0.02, suggesting post-depositional disturbance of the
284 isotope system, and are not considered further.

285

286 5. Discussion

287 The chemical and mineralogical composition of siliciclastic sedimentary rocks,
288 especially fine-grained rocks, are mainly controlled by the nature of their source rocks, and
289 they have been widely used in constraining the provenance, sedimentary processes, and
290 tectonic setting of sedimentary basins (Bhatia and Crook, 1986; Cullers, 2000, 1994; Large et
291 al., 2018; McLennan et al., 1993, 1990; Roser and Korsch, 1986). Most of the major elements
292 (e.g., Ca, Fe, Na, K, and Mg) have high solubility in water and easily fractionate during
293 sedimentary processes, making them unreliable as provenance proxies. Therefore, provenance
294 analysis typically relies on elements such as REE and certain HFSE such as Al, Ti, Th, Sc, Y,
295 and Zr because of their relative immobility during sedimentary processes and short residence

296 time in seawater (e.g., Taylor and McLennan, 1985; and references therein). However,
297 sedimentary processes such as grain sorting, chemical weathering, sedimentation, diagenesis,
298 and low-temperature alteration can result in significant changes to mineralogical and
299 geochemical composition compared to that of their original source (e.g., McLennan et al.,
300 1993, 2003; and references therein). In addition, enrichment in heavy minerals such as zircon,
301 monazite, and apatite during sedimentary transport can exert strong influence on trace element
302 and REE contents as they are preferentially concentrated in these minerals (e.g., McLennan et
303 al., 1993; Sugitani et al., 2006). These processes make it difficult to determine whether the
304 geochemical signatures preserved in siliciclastic sediments truly reflect the composition of the
305 provenance or were imprinted by sedimentary processes. It is therefore necessary to first
306 evaluate the influence of sedimentary processes on geochemical composition to resolve
307 primary signals from secondary overprints before using them in provenance analysis.

308

309 5.1 Sediment maturity, sorting, and mineral control

310 Concentrations of major element oxides and their ratios have been used to classify
311 sedimentary rocks and the $\text{SiO}_2/\text{Al}_2\text{O}_3$ ratio has been used to evaluate their maturity (e.g.,
312 Bhatia and Crook, 1986). Sediment maturity increases with increasing $\text{SiO}_2/\text{Al}_2\text{O}_3$ ratios
313 reflecting decrease in feldspar and clay content. The moderate to high $\text{SiO}_2/\text{Al}_2\text{O}_3$ ratios of the
314 FA Formation sandstones (Fig. 4) are typical of chemically immature to mature sandstones,
315 suggesting derivation of these sandstones from a range of proximal to distal source areas.
316 Furthermore, Th/Sc and Zr/Sc ratios provide insight into sediment recycling and heavy
317 mineral accumulation as both Th and Zr are incompatible elements, and are typically stronger
318 enriched in felsic rocks than the more compatible Sc (McLennan et al., 1993, 2003). The
319 average Th/Sc ratio is lower in the FB₁ Member mudstones (0.52-1.39; average = 0.86) than
320 FA Formation mudstones (0.98-3.36; average = 1.88) and sandstones (2.16-5.64; average =

321 3.85), indicating more evolved source for the FA Formation sediments compared to the FB₁
322 Member. Most of the FB₁ Member and FA Formation mudstones cluster close to the Late
323 Archean Upper Continental Crust (LAUCC), and provenance-dependent compositional
324 variation trend on the Th/Sc vs Zr/Sc diagram (Fig. 7), with limited spread along the zircon
325 addition trend, ruling out major role of hydraulic sorting and heavy mineral fractionation on
326 their chemical composition, and probably reflect chemical composition of their source rocks.
327 In contrast, the FA Formation sandstones and few FA Formation mudstones have elevated
328 Zr/Sc ratios, indicating significant zircon addition due to reworking and heavy-mineral
329 concentration (McLennan et al., 1993).

330 Trace elements, including REE, in siliciclastic rocks are generally hosted by clay
331 minerals and heavy minerals such as zircon, monazite, and apatite. Zircon is characterized by
332 enrichment in HREE relative to LREE, and this results in a negative correlation between Zr
333 and La_N/Yb_N (Yang et al., 1998). In contrast, monazite and apatite are preferentially enriched
334 in LREE and a negative correlation of Gd_N/Yb_N with Th and Gd_N/Yb_N with P₂O₅,
335 respectively, corresponds to their major contribution to sediment composition (McLennan,
336 1989). The moderately positive correlation of Al₂O₃ with \sum REE for all samples (Fig. 8a)
337 indeed demonstrates that REE are mostly hosted by aluminosilicates in the mudstones ($R^2 =$
338 0.57) and, to a lesser degree, in the sandstones ($R^2 = 0.27$), and positive correlation of \sum REE
339 with K₂O (Fig. 8b) suggests illite as the main carrier for REE in the mudstones ($R^2 = 0.59$)
340 and sandstones ($R^2 = 0.73$). Poor correlation between La_N/Yb_N and Zr for the FB₁ Member
341 mudstones ($R^2 = 0.06$), and FA Formation mudstones and sandstones ($R^2 = 0.14$) points to
342 limited influence of zircon as a carrier for REE, except for few samples of the FA Formation
343 (mostly sandstones) with elevated Zr content (Fig. 8c). Additionally, poor correlation between
344 Th and Gd_N/Yb_N (Fig. 8d) and between P₂O₅ and Gd_N/Yb_N (Fig. 8e) in the mudstones and
345 sandstones is inconsistent with phosphate enrichment (e.g., monazite and apatite) and does not

346 support significant control of these minerals over REE concentration, except for three FA
347 Formation sandstones with high Th content.

348

349 5.2 Post-depositional element mobility

350 Monazite is a common accessory mineral in the FA Formation, and Mathieu et al.
351 (2001) and Cuney and Mathieu (2000) showed that alteration of monazite crystals in the FA
352 Formation coarse-grained sandstones at the Oklo and Bangombe natural reactors by highly
353 saline diagenetic brines resulted in leaching and redistribution of LREEs. Using La as
354 representative of the LREEs and Th as an immobile element, the authors quantified LREEs
355 loss from the FA Formation coarse-grained sandstones due to monazite alteration by
356 comparing their Th/La ratios with the average values for Archean and Post-Archean
357 sandstones and shales. Cuney and Mathieu (2000) found that the whole-rock Th/La ratio
358 increased from 0.27 ± 0.2 in unaltered mudstones of the FA and FB formations to 1.14 ± 0.15 in
359 altered, coarse-grained sandstones of the FA Formation. Using similar approach, we evaluated
360 the post-depositional redistribution and remobilization of LREEs by comparing Th/La ratios
361 of the analyzed samples to the average values of Archean and Post-Archean shales (0.27 to
362 0.38) and sandstones (0.35 to 0.42) from Condie (1993). We used a Th/La ratio of 0.5 as an
363 alteration baseline, implying that samples with $\text{Th/La} \geq 0.5$ are altered and those having this
364 value below 0.5 are unaltered or minimally altered. The FB₁ Member and FA Formation
365 mudstones have low Th/La ratios similar to those of the Archean and Proterozoic shales, and
366 mostly plot in the unaltered field, indicating insignificant leaching of the LREE from the
367 mudstones, whereas most of the FA Formation sandstones have considerably higher Th/La
368 ratios and mostly plot in the altered field, likely reflecting more porous and permeable nature
369 of the sandstones and remobilization of LREEs (Fig. 8f).

370 Moreover, post-depositional alteration could potentially impact Sm-Nd isotope

371 composition because the Nd isotope system is not entirely immune to alteration, especially by
372 processes that mobilize REEs (e.g., Öhlander et al., 2000; Mathieu et al., 2001). For instance,
373 several studies (e.g., McLennan et al., 1993, 2003; Bock et al., 1994; Ehrenberg and Nadeau,
374 2002) have shown that positive correlation between Sm-Nd ratios and depleted mantle model
375 ages (T_{DM}) is an evidence for post-depositional disturbance of the Sm-Nd isotope system.
376 These studies have shown that an open-system behavior during diagenesis might result in
377 higher whole-rock Sm/Nd ratios and depleted mantle model ages. Excluding two outliers with
378 anomalously high $^{147}\text{Sm}/^{144}\text{Nd}$ ratios (Table 1), there is no apparent correlation between these
379 two parameters for the FA Formation sandstones ($R^2 = 0.04$) and FA Formation and FB₁
380 Member mudstones ($R^2 = 0.12$), suggesting that the Sm-Nd isotope system of these samples
381 was not disturbed after deposition. Furthermore, parallel chondrite-normalized REE patterns
382 with limited range in sample/chondrite ratio and lack of Ce anomaly displayed by all samples
383 (Fig. 6) support the relative immobility of the REE (cf. McLennan et al., 1993, 2003).
384 Overall, REE in most of the studied samples from the Franceville sub-basin do not appear to
385 be fractionated by sedimentary and post-depositional processes; and thus, geochemical and
386 isotope signatures of the Francevillian Group sediments, especially of the mudstones, were
387 largely preserved on the whole-rock scale. Effect of sorting and heavy mineral enrichment on
388 composition of the coarse-grained sandstones is further discussed below.

389

390 5.3 Paleoweathering of the source area

391 The intensity of weathering in source area can be assessed with the chemical index of
392 alteration (where $\text{CIA} = [(\text{Al}_2\text{O}_3 / (\text{Al}_2\text{O}_3 + \text{CaO}^* + \text{Na}_2\text{O} + \text{K}_2\text{O})) \times 100]$ in molar ratios and
393 CaO^* is the amount in silicate fraction; Nesbitt and Young, 1982), which measures the degree
394 of feldspar conversion to clays in shales during weathering. CIA values of unweathered to
395 weakly weathered rocks are close to 50 or less, moderately weathered rocks have values

396 between 60 and 80, and highly weathered rocks have values above 80 (Nesbitt and Young,
397 1984, 1982; Fedo et al., 1995). We do not have data for carbonate and apatite content, and
398 thus cannot correct for their Ca contents. Hence, we assumed in our calculations that moles of
399 silicate $\text{CaO} = \text{Na}_2\text{O}$ for samples with $\text{CaO} > \text{Na}_2\text{O}$ and accepted measured CaO value if CaO
400 $\leq \text{Na}_2\text{O}$ (cf. Jian et al., 2013; Roddaz et al., 2006). The analyzed mudstones generally have
401 moderate to high CIA values from 59 to 82 (Table A1), with majority of the samples falling
402 between the range of unweathered igneous rocks (45-55) and typical average shale (70-75),
403 suggesting moderate chemical weathering in the source areas.

404 The CIA proxy could be compromised by post-depositional addition of K, which is
405 common to aluminous clays, and this is commonly visualized on an Al_2O_3 -($\text{CaO}^* + \text{Na}_2\text{O}$)-
406 K_2O (A-CN-K) ternary plot (Nesbitt and Young, 1984; Fedo et al., 1995). On such diagram,
407 weathering products line up parallel to the A-CN side, while any deviation from this trend
408 towards the A-K side of the diagram indicates significant K addition (Fedo et al., 1995). The
409 FB_1 Member mudstones plot between the TTG and granite weathering trends, while the FA
410 Formation mudstones and sandstones scatter to the right of the weathering trend of the
411 average granite, towards the A-K side of the A-CN-K ternary plot (Fig. 9), which is
412 inconsistent with typical weathering pattern and suggests post-depositional K addition during
413 illitization (Fedo et al., 1995). To overcome the problem of K-addition, we calculated the
414 chemical index of weathering ($\text{CIW} = [(\text{Al}_2\text{O}_3)/(\text{Al}_2\text{O}_3 + \text{CaO}^* + \text{Na}_2\text{O}) \times 100]$; Harnois, 1988)
415 and plagioclase index of alteration ($\text{PIA} = [(\text{Al}_2\text{O}_3 - \text{K}_2\text{O})/(\text{Al}_2\text{O}_3 + \text{CaO}^* + \text{Na}_2\text{O} - \text{K}_2\text{O}) \times 100]$;
416 Fedo et al., 1995) to assess plagioclase alteration during chemical weathering in the source
417 area. The PIA and CIW values of unweathered rocks are close to 50 and values close to 100
418 indicate complete plagioclase breakdown. The PIA and CIW values are high for the FB_1 (80-
419 98) Member and most of the FA Formation mudstones (91-98) and sandstones (92-97),
420 suggesting moderate to intense plagioclase alteration in the source area. Few samples,

421 however, have values lower than 80 (Table A1). The high PIA and CIW values compared to
422 the CIA values attest that the succession has been strongly illitized after deposition.

423

424 5.4 Sediment provenance

425 5.4.1 Trace elements

426 The distribution of the least-mobile, incompatible (REEs, HFSE, Th, and Y) and
427 compatible (Sc, V, Ni, Cr, and Co) trace elements have been recognized to reflect the
428 composition of provenance and discriminate felsic from mafic source rocks (e.g., Taylor and
429 McLennan, 1985; Floyd and Leveridge, 1987; Cullers, 1994, 2000; McLennan et al., 1993;
430 Condie, 1993; Large et al., 2018). The incompatible elements are generally enriched in upper
431 continental crust felsic rocks and low in mafic and ultramafic mantle-derived rocks compared
432 to the compatible elements. The variable enrichments and depletions in incompatible and
433 compatible elements in the FA Formation and FB₁ Member mudstones (Fig. 5a-b) suggest a
434 mixed signature of felsic and mafic sources. In contrast, the FA Formation sandstones
435 strongly suggest a predominantly felsic source as they are mostly enriched in incompatible
436 elements and depleted in compatible elements with respect to LAUCC (Fig. 5c). Geochemical
437 discriminant diagrams such as Th/Sc versus Th/Cr (Fig. 10a) and Th/Sc versus La/Sc (Fig.
438 10b) show that all the samples, except for two FB₁ Member mudstones, have considerable
439 higher Th/Sc, La/Sc, and Th/Cr ratios than the LAUCC, plotting between granite and TTG
440 within the felsic provenance field on Figure 10b. However, the FB₁ Member mudstones have
441 lower Th/Sc, Th/Cr, La/Th, and La/Cr ratios and plot between TTG and mafic source field
442 (Fig. 10a), suggesting stronger mafic input compared to the FA Formation sediments. All
443 samples are characterized by low La/Th ratios and variable Hf content, and predominantly
444 plot within the felsic source and mixed felsic/mafic source fields on the La/Th versus Hf
445 diagram (Fig. 10c). The predominantly felsic composition of the provenance is supported by

446 the low Cr/V ratios and slightly variable Y/Ni ratios, which might reflect homogenous source
447 or efficient sediment mixing (Fig. 10d; cf. Ghosh et al., 2016).

448 In addition, distribution patterns of REE and the size of Eu anomaly have also been
449 used as proxies for determining the composition of the source area for siliciclastic
450 sedimentary rocks (e.g., Taylor and McLennan, 1985; Condie, 1993; Cullers, 1994, 2000).
451 The degree of LREE enrichment over HREE (La_N/Yb_N) measures the proportion of felsic to
452 mafic components with LREE enrichment being lower in mafic rocks compared to felsic
453 rocks, and the largest enrichment observed in TTG rocks. The size of Eu anomaly could
454 reflect intracrustal igneous differentiation, separating from the source magma granitic melts
455 and leaving behind residue with feldspar, which is the main host of Eu^{2+} in igneous rocks
456 (Taylor and McLennan, 1985; McLennan et al., 1993; 2003; Gao and Wedepohl, 1995;
457 Cullers, 2000). The seemingly similar chondrite-normalized REE patterns characterized by
458 high La_N/Yb_N ratios, relatively flat HREE, negative to negligible Eu anomalies, and negative
459 Ta and Nb suggest predominant derivation from granitoids for the FA Formation and FB₁
460 Member sediments. The distinctly negative Eu anomalies shown by most of the sediments,
461 especially by the FA Formation sandstones, can be attributed to fractionation induced by
462 feldspar-rich residuum during intracrustal fractionation in the provenance (cf. Gao and
463 Wedepohl, 1995), suggesting deposition of differentiated crust-derived sediments in stable
464 cratonic environment comparable to that for LAUCC (Ghosh et al., 2016). On another hand,
465 weakly positive to negligible Ta, Nb, and Eu anomalies in few of the FA Formation and FB₁
466 Member mudstones are potentially related to their higher feldspar (mostly plagioclase)
467 content (Table A3; cf. Taylor and McLennan, 1985; Bankole et al., 2015), which likely
468 reflects derivation from less differentiated mafic- and mantle-derived source rocks. Together,
469 these features point to heterogeneous provenance dominated by felsic, upper continental crust
470 materials.

471

472 5.4.2 Nd isotopes and crustal evolution

473 The Nd isotope composition can be used as an independent proxy to provide further
 474 constraint on the provenance for the Francevillian Group and its crustal residence age. The
 475 Sm-Nd isotope system is unique in provenance studies because both the parent (^{147}Sm) and
 476 daughter (^{143}Nd) isotopes are REE, and are highly immobile in sediments under most post-
 477 depositional processes and during low-temperature metamorphism. According to DePaolo and
 478 Wasserburg (1976), DePaolo et al. (1991), and McLennan and Hemming (1992), sedimentary
 479 rocks derived from less differentiated, mafic and juvenile sources in active tectonic settings
 480 commonly have high $^{143}\text{Nd}/^{144}\text{Nd}$ ratios, positive $\epsilon_{\text{Nd}(t)}$ values, variable and generally high
 481 Sm/Nd ratios, and low Th/Sc ratios (≤ 1). In contrast, those derived from old, upper
 482 continental crust in passive/cratonic settings are typically characterized by low $^{143}\text{Nd}/^{144}\text{Nd}$
 483 ratios, negative $\epsilon_{\text{Nd}(t)}$ values, low Sm/Nd ratios, and high Th/Sc ratios (≥ 1).

484 The analyzed FA Formation and FB₁ Member mudstones and sandstones all have
 485 almost invariably negative $\epsilon_{\text{Nd}(t)}$ and low $f^{\text{Sm}/\text{Nd}}$ values, uniform Sm/Nd ratios, and
 486 significantly higher and nearly uniform Th/Sc ratios (≥ 1), indicating dominance in the
 487 provenance of old, differentiated upper crust (Table 1; Figs. 11a-b). The data all scatter
 488 around grey TTG granitoids of the East Gabonian block, close to the upper continental crust
 489 end-member stretching from the Archean crust to volcanic arc rocks within the LREE-
 490 enriched field on the $f^{\text{Sm}/\text{Nd}}$ versus $\epsilon_{\text{Nd}(t)}$ diagram (Fig. 11b). Nd-isotope data for all the
 491 samples indicate overwhelming contribution of evolved and differentiated, older TTG-like
 492 upper continental crust in a passive margin setting on a stable craton.

493 According to the mixing model of DePaolo et al. (1991), the relative contribution of
 494 the Archean crustal (AC) material is given by: $\text{AC} = (1 - \alpha_{\text{VA}}) * 100$, where α_{VA} (contribution of
 495 the arc material) = $\beta^* / [(\epsilon_{\text{Nd}}\text{VA} - \epsilon_{\text{Nd}}\text{S}) / (\epsilon_{\text{Nd}}\text{S} - \epsilon_{\text{Nd}}\text{AC}) + \beta^*]$, β^* is the ratio of Nd concentration

496 in the volcanic arc rocks and Archean crust (Nd_{VA}/Nd_{AC}), ϵ_{NdVA} is the isotopic composition
497 of the volcanic arc component, ϵ_{NdS} is the isotopic composition of the analyzed rock, and
498 ϵ_{NdAC} is the isotopic composition of the Archean crust. We used the average values for the
499 Mesoarchean basement rocks around the Francevillian basin, $\epsilon_{NdAC} = -11.21$ and $Nd_{AC} =$
500 37.8 ppm (cf. Thiéblemont et al., 2009), for the Archean crust end-member, and $\epsilon_{NdVA} = 5$
501 and $Nd_{VA} = 10$ ppm for the volcanic arc end member. The mixing model results do not show
502 any trend with the stratigraphic position, and indicate that the detrital materials for the FA
503 Formation sandstones and mudstones and FB_1 Member mudstones were predominantly
504 derived from the older crystalline basement rocks with negligible to minor volcanic arc input
505 (Table 2). The geochemical provenance model is thus fully consistent with the results of the
506 LA-ICP-MS U-Pb study of detrital zircons from the FA and FB formations, which have
507 exclusively shown Neoproterozoic to Mesoarchean dates (Ossa Ossa et al., 2020).

508 The T_{DM} age range (2.73-3.05 Ga; Table 1) for all the samples is similar and consistent
509 with the U-Pb ages of detrital monazites (Mouélé et al., 2014) and zircons (Bankole et al.,
510 2018; Ossa Ossa et al., 2020) from the underlying crystalline basement rocks, suggesting that
511 the ca. 3.1 to 2.8 Ga granitoids of the East Gabonian block were the principal source for the
512 lower Francevillian Group sediments. The Mesoarchean basement rocks are composed of K-
513 rich granitoids (pink granite; monzogranite) and TTG granitoids with minor occurrences of
514 charnockites and the Belinga greenstone belts in places (Fig. 1). Although the trace element
515 geochemical proxies can separate contribution from felsic vs. mafic rocks in this study, they
516 cannot distinguish between the K-rich granite and TTG suite as the samples fall on the mixing
517 line within the felsic compositional field with basalt, TTG, and granite aligned along it (Figs.
518 10a-b). Trace element geochemical proxies for the FA Formation and FB_1 Member
519 sedimentary rocks show some similarity; however, it appears that most of the FA Formation
520 sandstones and mudstones have higher content of incompatible elements, more negative Eu

521 anomalies, and a relatively flat HREE pattern compared to the FB1 Member mudstones.
522 Therefore, it is likely that the FA Formation sedimentary rocks, especially the sandstones, had
523 larger contribution of intracrustally fractionated Mesoarchean K-rich granites than most of the
524 FB₁ Member mudstones, which are predominantly characterized by small negative to
525 negligible Eu anomalies and steeper HREE patterns (larger Gd/Yb ratios) (cf. McLennan et
526 al., 1990). This is in agreement with Ossa Ossa et al. (2020) who used detrital zircon
527 geochronology to argue that the Mesoarchean, K-rich (pink) granitoids were the main source
528 for the uranium-bearing sandstones of the lower FA Formation. However, minor contribution
529 from the Mesoarchean greenstone belts, hosting mafic rocks of the Belinga Group, and
530 charnockites is entirely possible. Lack of juvenile sources for the lower Francevillian Group
531 sediments, and the dominant Mesoarchean age (cf. Bankole et al., 2018; Ossa Ossa et al.,
532 2020) and relatively homogenous chemical composition of the provenance imply crustal
533 addition and effective recycling following magma extraction from the mantle between 2.73
534 and 3.05 Ga rather than formation of juvenile crust during deposition in the Francevillian
535 basin. Crustal recycling and mineralogical and geochemical fractionation via sedimentary
536 processes point at the existence of thick and stable continental crust during deposition of the
537 Francevillian Group on the Mesoarchean East Gabonian block.

538

539 5.5 Tectonic setting during deposition of the lower Francevillian Group

540 Geochemical discriminant diagrams using certain least-mobile trace elements have
541 been routinely used in resolving tectonic setting for sedimentary basins (e.g., Bhatia and
542 Crook, 1986; Roser and Korsch, 1988; McLennan et al., 1990; McLennan and Hemming,
543 1992; Cullers, 2000; Armstrong-Altrin et al., 2004; Schneiderhan et al., 2011). Although
544 many of these diagrams were defined for Phanerozoic sedimentary rocks, they have also been
545 applied to characterize tectonic setting of Precambrian sedimentary basins assuming that

546 plate-tectonic processes were active during this era. However, this approach sometimes results
547 in confusing outcome due to the control of the nature of the source rocks on geochemical
548 composition of sedimentary rocks (McLennan et al., 1993, 1990). On the La-Th-Sc ternary
549 discriminant diagram (Bhatia and Crook, 1986), the FA Formation and FB₁ Member
550 sediments predominantly fall within the passive margin (PM) and active continental margin
551 (ACM) fields (Fig. 12a). However, the FA Formation mudstones straddle the ACM and
552 Continental Island Arc (CIA) fields, while the FB₁ Member mudstones exclusively plot in the
553 CIA field on the Th-Sc-Zr/10 (Fig. 12b) and La/Y versus Sc/Cr discriminant diagrams (Fig.
554 12c). Although the FA Formation sandstones plot in the PM/ACM and PM fields on the La-
555 Th-Sc and Th-Sc-Zr/10 diagrams, respectively, they extend into the CIA field on the La/Y vs.
556 Sc/Cr diagram (Fig. 12c). Additionally, all the samples are characterized by variable low to
557 high Ti/Zr and La/Sc ratios, and therefore only few samples plot in the ACM, CIA, and PM
558 fields on Figure 12d, while the rest of the samples plots outside the discriminant fields on the
559 Ti/Zr vs. La/Sc diagram. The dominant contribution of older Archean crustal material and
560 lack of juvenile arc source make a CIA tectonic setting unlikely for the FA Formation and
561 FB₁ Member mudstones and sandstones. It seems likely that the CIA signature of sediments
562 might be caused by significant contribution of TTGs, which have similar trace element
563 geochemical signatures to those of CIA granitoids (cf. McLennan et al., 2006). Similarly, high
564 Ti/Zr ratios in most of the samples might reflect the predominantly Archean TTG provenance
565 to the sediments (cf. Martin et al., 2005). Hence, it is challenging to constrain a tectonic
566 setting using trace element composition for the Paleoproterozoic sedimentary basins, which
567 developed on the deeply eroded, Archean upper continental crust with predominantly
568 crystalline rocks in the provenance largely lacking contribution of recycled sedimentary
569 materials.

570

571 Conclusions

572 The whole-rock geochemistry and Nd isotope data for the unmetamorphosed, middle
573 Paleoproterozoic Francevillian Group FA Formation and FB₁ Member sediments demonstrate
574 that their geochemical signatures have not been considerably disturbed by sedimentary and
575 post-depositional processes and are thus suitable for the provenance study. The moderate
576 paleoweathering indices and position of the whole-rock geochemical data on the A-CN-K
577 ternary diagram suggest that the FA Formation sandstones and most of the FA Formation and
578 FB₁ Member mudstones have undergone significant chemical weathering and post-
579 depositional K addition. The geochemical signatures of selected relatively immobile elements,
580 including REE, and their ratios, and Nd isotope systematics indicate geochemically similar
581 sources for the FA Formation and FB₁ Member sediments that were predominantly derived
582 from the Mesoarchean TTGs of the East Gabonian block upper continental crust with only
583 minor, if any, mafic contribution from the Mesoarchean greenstone belts hosting the Belinga
584 Group. We infer that minimal to no contribution of juvenile arc materials to the middle
585 Paleoproterozoic Francevillian Group sediments is consistent with the recently inferred
586 foreland basin setting (Weber et al., 2016; Bankole et al., 2018; Ossa Ossa et al., 2020)
587 developed on the deeply eroded upper continental crust of the Mesoarchean East Gabonian
588 block.

589

590 Acknowledgements

591 The authors are grateful to the Gabonese Government, CENAREST, General
592 Direction of Mines and Geology, and *Agence Nationale des Parcs Nationaux* of Gabon for
593 logistic supports. This work was supported by *La Région Nouvelle Aquitaine*, France and
594 French Embassy in Libreville, Gabon. The authors would like to thank Prof. P. Mougouma

595 Daouda for his support. The authors also acknowledge Claude Fontaine, Claude Laforest,
 596 Cédric Lebailly, and Laurence Tromas for laboratory and administrative support at the
 597 University of Poitiers and David Vilbert for laboratory support at Rennes (GeOHeLis
 598 analytical facility). Participation of AB was made possible with the funding from the NSERC
 599 Discovery and Accelerator grants. We thank the editor, Axel Hoffman, and two anonymous
 600 reviewers for their constructive suggestions and comments.

601

602 **References**

- 603 Armstrong-Altrin, J.S., Lee, Y.I., Verma, S.P., Ramasamy, S., 2004. Geochemistry of Sandstones from
 604 the Upper Miocene Kudankulam Formation, Southern India: Implications for Provenance,
 605 Weathering, and Tectonic Setting. *J. Sediment. Res.* 74, 285–297.
 606 <https://doi.org/10.1306/082803740285>
- 607 Aubineau, J., Albani, A.E., Fru, E.C., Gingras, M., Batonneau, Y., Buatois, L.A., Geffroy, C., Labanowski,
 608 J., Laforest, C., Lemée, L., Mángano, M.G., Meunier, A., Pierson-Wickmann, A.-C., Recourt, P.,
 609 Riboulleau, A., Trentesaux, A., Konhauser, K.O., 2018. Unusual microbial mat-related
 610 structural diversity 2.1 billion years ago and implications for the Francevillian biota.
 611 *Geobiology* 16, 476–497. <https://doi.org/10.1111/gbi.12296>
- 612 Azzibrouck-Azziley, G., 1986. Sédimentologie et géochimie du Francevillien B (Protérozoïque
 613 inférieur), in: Métallogénie des gisements de manganèse de Moanda, Gabon. Université de
 614 Strasbourg, Strasbourg, France.
- 615 Bankole, O.M., Albani, A.E., Meunier, A., Pambo, F., Paquette, J.-L., Bekker, A., 2018. Earth's oldest
 616 preserved K-bentonites in the ca. 2.1 Ga Francevillian Basin, Gabon. *Am. J. Sci.* 318, 409–434.
 617 <https://doi.org/10.2475/04.2018.02>
- 618 Bankole, O.M., Albani, A.E., Meunier, A., Rouxel, O.J., Gauthier-Lafaye, F., Bekker, A., 2016. Origin of
 619 red beds in the Paleoproterozoic Franceville Basin, Gabon, and implications for sandstone-
 620 hosted uranium mineralization. *Am. J. Sci.* 316, 839–872. <https://doi.org/10.2475/09.2016.02>
- 621 Bankole, O.M., El Albani, A., Meunier, A., Gauthier-Lafaye, F., 2015. Textural and paleo-fluid flow
 622 control on diagenesis in the Paleoproterozoic Franceville Basin, South Eastern, Gabon.
 623 *Precambrian Res.* 268, 115–134. <https://doi.org/10.1016/j.precamres.2015.07.008>
- 624 Bekker, A., Sial, A.N., Karhu, J.A., Ferreira, V.P., Noce, C.M., Kaufman, A.J., Romano, A.W., Pimentel,
 625 M.M., 2003. Chemostratigraphy of Carbonates from the Minas Supergroup, Quadrilatero
 626 Ferrífero (Iron Quadrangle), Brazil: A Stratigraphic Record of Early Proterozoic Atmospheric,
 627 Biogeochemical and Climactic Change. *Am. J. Sci.* 303, 865–904.
 628 <https://doi.org/10.2475/ajs.303.10.865>
- 629 Bhatia, M.R., Crook, K.A.W., 1986. Trace element characteristics of graywackes and tectonic setting
 630 discrimination of sedimentary basins. *Contrib. Mineral. Petrol.* 92, 181–193.
 631 <https://doi.org/10.1007/BF00375292>
- 632 Bock, B., McLennan, S.M., Hanson, G.N., 1994. Rare earth element redistribution and its effects on
 633 the neodymium isotope system in the austin Glen Member of the Normanskill Formation,
 634 New York, USA. *Geochim. Cosmochim. Acta* 58, 5245–5253. [https://doi.org/10.1016/0016-7037\(94\)90308-5](https://doi.org/10.1016/0016-7037(94)90308-5)
- 635
 636 Bonhomme, M.G., Gauthier-Lafaye, F., Weber, F., 1982. An example of lower proterozoic sediments:
 637 The Francevillian in Gabon. *Precambrian Res.*, Geochronological correlation of Precambrian

- 638 sediments and volcanics in stable zones 18, 87–102. [https://doi.org/10.1016/0301-9268\(82\)90038-9](https://doi.org/10.1016/0301-9268(82)90038-9)
- 639
- 640 Bouton, P., Thiéblemont, D., Gouin, J., Cocherie, A., Guerrot, C., Tegye, M., Préat, A., Simo Ndounze, S., Moussavou, M., 2009. Notice explicative de la carte géologique de la République du Gabon à 1/200 000, feuille Franceville-Boumango. Edition DGMG-Ministère des Mines, du Pétrole, des Hydrocarbures, Libreville, Gabon.
- 641
- 642
- 643
- 644 Bros, R., Stille, P., Gauthier-Lafaye, F., Weber, F., Clauer, N., 1992. Sm-Nd isotopic dating of Proterozoic clay material: An example from the Francevillian sedimentary series, Gabon. *Earth Planet. Sci. Lett.* 113, 207–218. [https://doi.org/10.1016/0012-821X\(92\)90220-P](https://doi.org/10.1016/0012-821X(92)90220-P)
- 645
- 646
- 647 Caen-Vachette, M., Vialette, Y., Bassot, J., P., Vidal, P., 1988. Apport de la géochronologie isotopique à la connaissance de la géologie gabonaise (No. 491), *Chronique de la Recherche Minière*.
- 648
- 649 Canfield, D.E., Ngombi-Pemba, L., Hammarlund, E.U., Bengtson, S., Chaussidon, M., Gauthier-Lafaye, F., Meunier, A., Riboulleau, A., Rollion-Bard, C., Rouxel, O., Asael, D., Pierson-Wickmann, A.-C., Albani, A.E., 2013. Oxygen dynamics in the aftermath of the Great Oxidation of Earth's atmosphere. *Proc. Natl. Acad. Sci.* 110, 16736–16741. <https://doi.org/10.1073/pnas.1315570110>
- 650
- 651
- 652
- 653
- 654 Carignan, J., Hild, P., Mevelle, G., Morel, J., Yeghicheyan, D., 2001. Routine Analyses of Trace Elements in Geological Samples using Flow Injection and Low Pressure On-Line Liquid Chromatography Coupled to ICP-MS: A Study of Geochemical Reference Materials BR, DR-N, UB-N, AN-G and GH. *Geostand. Newsl.* 25, 187–198. <https://doi.org/10.1111/j.1751-908X.2001.tb00595.x>
- 655
- 656
- 657
- 658
- 659 Condie, K.C., 1993. Chemical composition and evolution of the upper continental crust: contrasting results from surface samples and shales. *Chem. Geol.* 104, 1–37.
- 660
- 661 Cullers, R., 2000. Geochemistry of the Mesoproterozoic Lakhanda shales in southeastern Yakutia, Russia: implications for mineralogical and provenance control, and recycling. *Precambrian Res.* 104, 77–93. [https://doi.org/10.1016/S0301-9268\(00\)00090-5](https://doi.org/10.1016/S0301-9268(00)00090-5)
- 662
- 663
- 664 Cullers, R.L., 1994. The controls on the major and trace element variation of shales, siltstones, and sandstones of Pennsylvanian-Permian age from uplifted continental blocks in Colorado to platform sediment in Kansas, USA. *Geochim. Cosmochim. Acta* 58, 4955–4972. [https://doi.org/10.1016/0016-7037\(94\)90224-0](https://doi.org/10.1016/0016-7037(94)90224-0)
- 665
- 666
- 667
- 668 Cuney, M., Mathieu, R., 2000. Extreme light rare earth element mobilization by diagenetic fluids in the geological environment of the Oklo natural reactor zones, Franceville basin, Gabon. *Geology* 28, 743–746. [https://doi.org/10.1130/0091-7613\(2000\)28<743:ELREEM>2.0.CO;2](https://doi.org/10.1130/0091-7613(2000)28<743:ELREEM>2.0.CO;2)
- 669
- 670
- 671 DePaolo, D.J., Linn, A.M., Schubert, G., 1991. The continental crustal age distribution: Methods of determining mantle separation ages from Sm-Nd isotopic data and application to the southwestern United States. *J. Geophys. Res. Solid Earth* 96, 2071–2088. <https://doi.org/10.1029/90JB02219>
- 672
- 673
- 674
- 675 DePaolo, D.J., Wasserburg, G.J., 1976. Inferences about magma sources and mantle structure from variations of ¹⁴³Nd/¹⁴⁴Nd. *Geophys. Res. Lett.* 3, 743–746. <https://doi.org/10.1029/GL003i012p00743>
- 676
- 677
- 678 Ehrenberg, S.N., Nadeau, P.H., 2002. Postdepositional Sm/Nd Fractionation in Sandstones: Implications for Neodymium-Isotope Stratigraphy. *J. Sediment. Res.* 72, 304–315. <https://doi.org/10.1306/060901720304>
- 679
- 680
- 681 El Albani, A., Bengtson, S., Canfield, D.E., Riboulleau, A., Bard, C.R., Macchiarelli, R., Pemba, L.N., Hammarlund, E., Meunier, A., Mouele, I.M., Benzerara, K., Bernard, S., Boulvais, P., Chaussidon, M., Cesari, C., Fontaine, C., Chi-Fru, E., Ruiz, J.M.G., Gauthier-Lafaye, F., Mazurier, A., Pierson-Wickmann, A.C., Rouxel, O., Trentesaux, A., Vecoli, M., Versteegh, G.J.M., White, L., Whitehouse, M., Bekker, A., 2014. The 2.1 Ga Old Francevillian Biota: Biogenicity, Taphonomy and Biodiversity. *PLOS ONE* 9, e99438. <https://doi.org/10.1371/journal.pone.0099438>
- 682
- 683
- 684
- 685
- 686
- 687
- 688 El Albani, A., Mangano, M.G., Buatois, L.A., Bengtson, S., Riboulleau, A., Bekker, A., Konhauser, K., Lyons, T., Rollion-Bard, C., Bankole, O., Baghekema, S.G.L., Meunier, A., Trentesaux, A.,
- 689

- 690 Mazurier, A., Aubineau, J., Laforest, C., Fontaine, C., Recourt, P., Fru, E.C., Macchiarelli, R.,
691 Reynaud, J.Y., Gauthier-Lafaye, F., Canfield, D.E., 2019. Organism motility in an oxygenated
692 shallow-marine environment 2.1 billion years ago. *Proc. Natl. Acad. Sci.* 116, 3431–3436.
693 <https://doi.org/10.1073/pnas.1815721116>
- 694 Fedo, C.M., Nesbitt, H.W., Young, G.M., 1995. Unraveling the effects of potassium metasomatism in
695 sedimentary rocks and paleosols, with implications for paleoweathering conditions and
696 provenance. *Geology* 23, 921–924. [https://doi.org/10.1130/0091-
697 7613\(1995\)023<0921:UTEOPM>2.3.CO;2](https://doi.org/10.1130/0091-7613(1995)023<0921:UTEOPM>2.3.CO;2)
- 698 Feybesse, J.L., Johan, V., Triboulet, C., Guerrot, C., Mayaga-Mikolo, F., Bouchot, V., Eko N'dong, J.,
699 1998. The West Central African belt: a model of 2.5–2.0Ga accretion and two-phase orogenic
700 evolution. *Precambrian Res.* 87, 161–216. [https://doi.org/10.1016/S0301-9268\(97\)00053-3](https://doi.org/10.1016/S0301-9268(97)00053-3)
- 701 Floyd, P.A., Leveridge, B.E., 1987. Tectonic environment of the Devonian Gramscatho basin, south
702 Cornwall: framework mode and geochemical evidence from turbiditic sandstones. *J. Geol.*
703 *Soc.* 144, 531–542. <https://doi.org/10.1144/gsjgs.144.4.0531>
- 704 Gao, S., Wedepohl, K.H., 1995. The negative Eu anomaly in Archean sedimentary rocks: Implications
705 for decomposition, age and importance of their granitic sources. *Earth Planet. Sci. Lett.* 133,
706 81–94. [https://doi.org/10.1016/0012-821X\(95\)00077-P](https://doi.org/10.1016/0012-821X(95)00077-P)
- 707 Gauthier-Lafaye, F., 2006. Time constraint for the occurrence of uranium deposits and natural
708 nuclear fission reactors in the Paleoproterozoic Franceville Basin (Gabon). *Geol. Soc. Am.*
709 *Mem.* 198, 157–167. <https://doi.org/10.1130/2006.1198>
- 710 Gauthier-Lafaye, F., 1986. Les gisements d'uranium du Gabon et les reacteurs d'Oklo. Modèle
711 métallogénique de gîtes à fortes teneurs du protérozoïque inférieur. Université de
712 Strasbourg, Strasbourg, France.
- 713 Gauthier-Lafaye, F., Weber, F., 2003. Natural nuclear fission reactors: time constraints for
714 occurrence, and their relation to uranium and manganese deposits and to the evolution of
715 the atmosphere. *Precambrian Res.* 120, 81–100. [https://doi.org/10.1016/S0301-
716 9268\(02\)00163-8](https://doi.org/10.1016/S0301-9268(02)00163-8)
- 717 Gauthier-Lafaye, F., Weber, F., 1989. The Francevillian (Lower Proterozoic) uranium ore deposits of
718 Gabon. *Econ. Geol.* 84, 2267–2285. <https://doi.org/10.2113/gsecongeo.84.8.2267>
- 719 Ghosh, S., De, S., Mukhopadhyay, J., 2016. Provenance of >2.8 Ga Keonjhar Quartzite, Singhbhum
720 Craton, Eastern India: Implications for the Nature of Mesoarchean Upper Crust and
721 Geodynamics. *J. Geol.* 124, 331–351. <https://doi.org/10.1086/685862>
- 722 Grisolia, M.F.P., Oliveira, E.P., 2012. Sediment provenance in the Palaeoproterozoic Rio Itapicuru
723 greenstone belt, Brazil, indicates deposition on arc settings with a hidden 2.17–2.25Ga
724 substrate. *J. South Am. Earth Sci.* 38, 89–109. <https://doi.org/10.1016/j.jsames.2012.06.004>
- 725 Harnois, L., 1988. The CIW index: A new chemical index of weathering. *Sediment. Geol.* 55, 319–322.
726 [https://doi.org/10.1016/0037-0738\(88\)90137-6](https://doi.org/10.1016/0037-0738(88)90137-6)
- 727 Haubensack, C., 1981. Environnement des grès protérozoïques et des indices uranifères du secteur
728 Kiéné dans le bassin de Franceville (République Gabonaise): Aspects sédimentologiques et
729 géochimiques. Université de Strasbourg, Strasbourg, France.
- 730 Herron, M.M., 1988. Geochemical Classification of Terrigenous Sands and Shales from Core or Log
731 Data. *J. Sediment. Res.* 58, 820–829.
- 732 Horie, K., Hidaka, H., Gauthier-Lafaye, F., 2005. U-Pb Zircon geochronology of the Franceville series at
733 Bidoudouma, Gabon. Presented at the Goldschmidt Conference Abstract, *Geochimica et*
734 *Cosmochimica Acta*, p. A11.
- 735 Jian, X., Guan, P., Zhang, W., Feng, F., 2013. Geochemistry of Mesozoic and Cenozoic sediments in
736 the northern Qaidam basin, northeastern Tibetan Plateau: Implications for provenance and
737 weathering. *Chem. Geol.* 360–361, 74–88. <https://doi.org/10.1016/j.chemgeo.2013.10.011>
- 738 Karhu, J.A., Holland, H.D., 1996. Carbon isotopes and the rise of atmospheric oxygen. *Geology* 24,
739 867–870. [https://doi.org/10.1130/0091-7613\(1996\)024<0867:CIATRO>2.3.CO;2](https://doi.org/10.1130/0091-7613(1996)024<0867:CIATRO>2.3.CO;2)

- 740 Kump, L.R., Junium, C., Arthur, M.A., Brasier, A., Fallick, A., Melezhik, V., Lepland, A., CČrne, A.E., Luo,
741 G., 2011. Isotopic Evidence for Massive Oxidation of Organic Matter Following the Great
742 Oxidation Event. *Science* 334, 1694–1696. <https://doi.org/10.1126/science.1213999>
- 743 Large, R.R., Mukherjee, I., Zhukova, I., Corkrey, R., Stepanov, A., Danyushevsky, L.V., 2018. Role of
744 upper-most crustal composition in the evolution of the Precambrian ocean–atmosphere
745 system. *Earth Planet. Sci. Lett.* 487, 44–53. <https://doi.org/10.1016/j.epsl.2018.01.019>
- 746 Ledru, P., Eko N'Dong, J., Johan, V., Prian, J.-P., Coste, B., Haccard, D., 1989. Structural and
747 metamorphic evolution of the Gabon Orogenic Belt: Collision tectonics in the lower
748 proterozoic? *Precambrian Res.* 44, 227–241. [https://doi.org/10.1016/0301-9268\(89\)90046-6](https://doi.org/10.1016/0301-9268(89)90046-6)
- 749 Maheshwari, A., Sial, A.N., Gaucher, C., Bossi, J., Bekker, A., Ferreira, V.P., Romano, A.W., 2010.
750 Global nature of the Paleoproterozoic Lomagundi carbon isotope excursion: A review of
751 occurrences in Brazil, India, and Uruguay. *Precambrian Res., Precambrian Isotope*
752 *Stratigraphy* 182, 274–299. <https://doi.org/10.1016/j.precamres.2010.06.017>
- 753 Martin, A.P., Condon, D.J., Prave, A.R., Lepland, A., 2013. A review of temporal constraints for the
754 Palaeoproterozoic large, positive carbonate carbon isotope excursion (the Lomagundi–Jatuli
755 Event). *Earth-Sci. Rev.* 127, 242–261. <https://doi.org/10.1016/j.earscirev.2013.10.006>
- 756 Martin, A.P., Prave, A.R., Condon, D.J., Lepland, A., Fallick, A.E., Romashkin, A.E., Medvedev, P.V.,
757 Rychanchik, D.V., 2015. Multiple Palaeoproterozoic carbon burial episodes and excursions.
758 *Earth Planet. Sci. Lett.* 424, 226–236. <https://doi.org/10.1016/j.epsl.2015.05.023>
- 759 Martin, H., Smithies, R.H., Rapp, R., Moyen, J.-F., Champion, D., 2005. An overview of adakite,
760 tonalite–trondhjemite–granodiorite (TTG), and sanukitoid: relationships and some
761 implications for crustal evolution. *Lithos* 79, 1–24.
762 <https://doi.org/10.1016/j.lithos.2004.04.048>
- 763 Mathieu, R., Zetterström, L., Cuney, M., Gauthier-Lafaye, F., Hidaka, H., 2001. Alteration of monazite
764 and zircon and lead migration as geochemical tracers of fluid paleocirculations around the
765 Oklo–Okélobondo and Bangombé natural nuclear reaction zones (Franceville basin, Gabon).
766 *Chem. Geol.* 171, 147–171. [https://doi.org/10.1016/S0009-2541\(00\)00245-X](https://doi.org/10.1016/S0009-2541(00)00245-X)
- 767 McDonough, W.F., Sun, S. -s., 1995. The composition of the Earth. *Chem. Geol., Chemical Evolution*
768 *of the Mantle* 120, 223–253. [https://doi.org/10.1016/0009-2541\(94\)00140-4](https://doi.org/10.1016/0009-2541(94)00140-4)
- 769 McLennan, S.M., 1989. Rare earth elements in sedimentary rocks; influence of provenance and
770 sedimentary processes. *Rev. Mineral. Geochem.* 21, 169–200.
- 771 McLennan, S.M., Bock, B., Hemming, S.R., Hurowitz, J.A., Lev, S.M., McDaniel, D.K., 2003. The roles of
772 provenance and sedimentary processes in the geochemistry of sedimentary rocks, in:
773 *Geochemistry of Sediments and Sedimentary Rocks: Evolutionary Considerations to Mineral*
774 *Deposit-Forming Environments.* Geological Association of Canada, pp. 7–38.
- 775 McLennan, S.M., Hemming, S., 1992. Samarium/neodymium elemental and isotopic systematics in
776 sedimentary rocks. *Geochim. Cosmochim. Acta* 56, 887–898. [https://doi.org/10.1016/0016-7037\(92\)90034-G](https://doi.org/10.1016/0016-7037(92)90034-G)
- 777
778 McLennan, S.M., Hemming, S., McDaniel, D.K., Hanson, G.N., 1993. Geochemical approaches to
779 sedimentation, provenance, and tectonics, in: *Geological Society of America Special Papers.*
780 *Geological Society of America*, pp. 21–40. <https://doi.org/10.1130/SPE284-p21>
- 781 McLennan, S.M., Taylor, S.R., Hemming, S., R., 2006. Composition, differentiation, and evolution of
782 continental crust: Constraints from sedimentary rocks and heat flow, in: *Evolution and*
783 *Differentiation of the Continental Crust.* Cambridge Univ. Press, pp. 92–134.
- 784 McLennan, S.M., Taylor, S.R., McCulloch, M.T., Maynard, J.B., 1990. Geochemical and Nd–Sr isotopic
785 composition of deep-sea turbidites: Crustal evolution and plate tectonic associations.
786 *Geochim. Cosmochim. Acta* 54, 2015–2050. [https://doi.org/10.1016/0016-7037\(90\)90269-Q](https://doi.org/10.1016/0016-7037(90)90269-Q)
- 787 Mouélé, I.M., Dudoignon, P., El Albani, A., Meunier, A., Boulvais, P., Gauthier-Lafaye, F., Paquette, J.-
788 L., Martin, H., Cuney, M., 2014. 2.9–1.9Ga paleoalterations of Archean granitic basement of
789 the Franceville basin (Gabon). *J. Afr. Earth Sci.* 97, 244–260.
790 <https://doi.org/10.1016/j.jafrearsci.2014.04.027>

- 791 Nesbitt, H.W., Young, G.M., 1984. Prediction of some weathering trends of plutonic and volcanic
792 rocks based on thermodynamic and kinetic considerations. *Geochim. Cosmochim. Acta* 48,
793 1523–1534. [https://doi.org/10.1016/0016-7037\(84\)90408-3](https://doi.org/10.1016/0016-7037(84)90408-3)
- 794 Nesbitt, H.W., Young, G.M., 1982. Early Proterozoic climates and plate motions inferred from major
795 element chemistry of lutites. *Nature* 299, 715–717. <https://doi.org/10.1038/299715a0>
- 796 Ngombi-Pemba, L., Albani, A.E., Meunier, A., Grauby, O., Gauthier-Lafaye, F., 2014. From detrital
797 heritage to diagenetic transformations, the message of clay minerals contained within shales
798 of the Palaeoproterozoic Francevillian basin (Gabon). *Precambrian Res.* 255, 63–76.
799 <https://doi.org/10.1016/j.precamres.2014.09.016>
- 800 Öhlander, B., Ingri, J., Land, M., Schöberg, H., 2000. Change of Sm-Nd isotope composition during
801 weathering of till. *Geochim. Cosmochim. Acta* 64, 813–820. [https://doi.org/10.1016/S0016-7037\(99\)00365-8](https://doi.org/10.1016/S0016-7037(99)00365-8)
- 803 Oliveira, E.P., McNaughton, N.J., Armstrong, R., 2010. Mesoarchaeon to Palaeoproterozoic growth of
804 the northern segment of the Itabuna–Salvador–Curaçá orogen, São Francisco craton, Brazil.
805 *Geol. Soc. Lond. Spec. Publ.* 338, 263–286. <https://doi.org/10.1144/SP338.13>
- 806 Ossa Ossa, F., Eickmann, B., Hofmann, A., Planavsky, N.J., Asael, D., Pambo, F., Bekker, A., 2018. Two-
807 step deoxygenation at the end of the Paleoproterozoic Lomagundi Event. *Earth Planet. Sci.*
808 *Lett.* 486, 70–83. <https://doi.org/10.1016/j.epsl.2018.01.009>
- 809 Ossa Ossa, F., Hofmann, A., Ballouard, C., Voster, C., Schoenberg, R., Fiedrich, A., Mayaga-Mikolo, F.,
810 Bekker, A., 2020. Constraining provenance for the uraniferous Paleoproterozoic Francevillian
811 Group sediments (Gabon) with detrital zircon geochronology and geochemistry. *Precambrian*
812 *Res.* 105724. <https://doi.org/10.1016/j.precamres.2020.105724>
- 813 Ovchinnikova, G.V., Kuznetsov, A.B., Melezhik, V.A., Gorokhov, I.M., Vasil'eva, I.M., Gorokhovskii,
814 B.M., 2007. Pb-Pb age of Jatulian carbonate rocks: The Tulomozero Formation of southeast
815 Karelia. *Stratigr. Geol. Correl.* 15, 359–372. <https://doi.org/10.1134/S0869593807040028>
- 816 Pambo, F., 2004. Conditions de formation des carbonates de manganese Proterozoïques et analyse
817 mineralogy et geochimiques des minerals a bioxydes de manganese associes dans le
818 gisement de Moanda, Sud-Est, Gabon. Université de Strasbourg, Strasbourg, France.
- 819 Préat, A., Bouton, P., Thiéblemont, D., Prian, J.-P., Ndounze, S.S., Delpomdor, F., 2011.
820 Paleoproterozoic high $\delta^{13}\text{C}$ dolomites from the Lastoursville and Franceville basins (SE
821 Gabon): Stratigraphic and syndimentary subsidence implications. *Precambrian Res.* 189,
822 212–228. <https://doi.org/10.1016/j.precamres.2011.05.013>
- 823 Reis, L.A., Martins-Neto, M.A., Gomes, N.S., Endo, I., Jordt-Evangelista, H., 2002. A BACIA DE
824 ANTEPAÍS PALEOPROTEROZÓICA SABARÁ, QUADRILÁTERO FERRÍFERO, MINAS GERAIS. *Rev.*
825 *Bras. Geociências* 32, 27–42.
- 826 Reynaud, J.-Y., Trentesaux, A., Albani, A.E., Aubineau, J., Ngombi-Pemba, L., Guiyeligou, G., Bouton,
827 P., Gauthier-Lafaye, F., Weber, F., 2017. Depositional setting of the 2.1 Ga Francevillian
828 macrobiota (Gabon): Rapid mud settling in a shallow basin swept by high-density sand flows.
829 *Sedimentology* 65, 670–701. <https://doi.org/10.1111/sed.12398>
- 830 Roddaz, M., Viers, J., Brusset, S., Baby, P., Boucayrand, C., Hérail, G., 2006. Controls on weathering
831 and provenance in the Amazonian foreland basin: Insights from major and trace element
832 geochemistry of Neogene Amazonian sediments. *Chem. Geol.* 226, 31–65.
833 <https://doi.org/10.1016/j.chemgeo.2005.08.010>
- 834 Rollison, H., 1993. Using geochemical data: evaluation, presentation, interpretation. Longman.
- 835 Roser, B.P., Korsch, R.J., 1988. Provenance signatures of sandstone-mudstone suites determined
836 using discriminant function analysis of major-element data. *Chem. Geol.* 67, 119–139.
837 [https://doi.org/10.1016/0009-2541\(88\)90010-1](https://doi.org/10.1016/0009-2541(88)90010-1)
- 838 Roser, B.P., Korsch, R.J., 1986. Determination of Tectonic Setting of Sandstone-Mudstone Suites
839 Using SiO_2 Content and $\text{K}_2\text{O}/\text{Na}_2\text{O}$ Ratio. *J. Geol.* 94, 635–650.
840 <https://doi.org/10.1086/629071>
- 841 Sawaki, Y., Moussavou, M., Sato, T., Suzuki, K., Ligna, C., Asanuma, H., Sakata, S., Obayashi, H., Hirata,
842 T., Edou-Minko, A., 2017. Chronological constraints on the Paleoproterozoic Francevillian

- 843 Group in Gabon. *Geosci. Front., Frontiers in Early Earth History and Primordial Life- Part I* 8,
844 397–407. <https://doi.org/10.1016/j.gsf.2016.10.001>
- 845 Schneiderhan, E., Zimmermann, U., Gutzmer, J., Mezger, K., Armstrong, R., 2011. Sedimentary
846 Provenance of the Neoproterozoic Ventersdorp Supergroup, Southern Africa: Shedding Light on
847 the Evolution of the Kaapvaal Craton during the Neoproterozoic. *J. Geol.* 119, 575–596.
848 <https://doi.org/10.1086/661988>
- 849 Sugitani, K., Yamashita, F., Nagaoka, T., Yamamoto, K., Minami, M., Mimura, K., Suzuki, K., 2006.
850 Geochemistry and sedimentary petrology of Archean clastic sedimentary rocks at Mt.
851 Goldsworthy, Pilbara Craton, Western Australia: Evidence for the early evolution of
852 continental crust and hydrothermal alteration. *Precambrian Res.* 147, 124–147.
853 <https://doi.org/10.1016/j.precamres.2006.02.006>
- 854 Taylor, S.R., McLennan, S.M., 1985. *The continental crust: Its evolution and composition.* Blackwell.
- 855 Thiéblemont, D., Bouton, P., Pr at, A., Goujou, J.-C., Tegye, M., Weber, F., Ebang Obiang, M., Joron,
856 J.L., Treuil, M., 2014. Transition from alkaline to calc-alkaline volcanism during evolution of
857 the Paleoproterozoic Francevillian basin of eastern Gabon (Western Central Africa). *J. Afr.*
858 *Earth Sci., Special Volume of the 24th Colloquium of African Geology* 99, 215–227.
859 <https://doi.org/10.1016/j.jafrearsci.2013.12.007>
- 860 Thiéblemont, D., Castaing, C., Billa, M., Bouton, P., Pr at, A., 2009. Notice explicative de la carte
861 g ologique et des ressources min rales de la R publique Gabonaise.
- 862 Weber, F., 1968. Une s rie pr cambrienne du Gabon: le Francevillien, s dimentologie, g ochimie,
863 relations avec les g tes min raux. Universit  de Strasbourg, Strasbourg, France.
- 864 Weber, F., Gauthier-Lafaye, F., Whitechurch, H., Ulrich, M., El Albani, A., 2016. The 2-Ga Eburnean
865 Orogeny in Gabon and the opening of the Francevillian intracratonic basins: A review.
866 *Comptes Rendus Geosci.* 348, 572–586. <https://doi.org/10.1016/j.crte.2016.07.003>
- 867 Yang, H., Kyser, K., Ansdell, K., 1998. Geochemical and Nd isotopic compositions of the
868 metasedimentary rocks in the La Ronge Domain, Trans-Hudson Orogen, Canada: implications
869 for evolution of the domain. *Precambrian Res.* 92, 37–64. [https://doi.org/10.1016/S0301-](https://doi.org/10.1016/S0301-9268(98)00067-9)
870 [9268\(98\)00067-9](https://doi.org/10.1016/S0301-9268(98)00067-9)

872 List of figures

- 873 Figure 1. Geological map of Gabon showing distribution of the Francevillian Group and the
874 Franceville sub-basin on the inset (modified from Thi blemont et al., 2009).
- 875 Figure 2. A. Geological map of Franceville sub-basin showing location of the drill cores
876 (modified from Aubineau et al., 2018) and (B) Lithostratigraphic column of the
877 Francevillian Group in the Franceville sub-basin, Gabon (modified from Weber,
878 1968). Sources of geochronologic age constraints: ¹- Horie et al., 2005; ²- Bonhomme
879 et al., 1982; ³- Bros et al., 1992; ⁴- Bouton et al., 2009.
- 880 Figure 3. Lithostratigraphy of the studied drill cores in the Franceville sub-basin showing

881 position of the studied samples. Two additional drill cores (BA 74 and GR 3), located
882 on Figure 2, are not shown on this figure since only partial drill core logs are available
883 for them and only three samples with well-defined stratigraphic positions from these
884 two drill cores were used in our study.

885 Figure 4. Geochemical classification of FA Formation and FB₁ Member sandstones and
886 mudstones (Herron, 1988).

887 Figure 5. Trace element spider diagrams for (A) FB₁ Member mudstones, (B) FA Formation
888 mudstones, and (C) FA Formation sandstones normalized to the composition of the
889 LAUCC (Late Archean Upper Continental Crust) from Condie (1993).

890 Figure 6. Chondrite-normalized Rare Earth Element (REE) patterns for (A) FB₁ Member
891 mudstones, (B) FA Formation mudstones, and (C) FA Formation sandstones,
892 compared with the Late Archean Upper Continental Crust (LAUCC) from Condie
893 (1993). Chondrite values are from McDonough and Sun (1995).

894 Figure 7. Plot of Th/Sc versus Zr/Sc for the studied Francevillian Group sediments (after
895 McLennan et al., 1993). Data for basalt, TTG (tonalite-trondhjemite-granodiorite),
896 granite, and LAUCC (Late Archean Upper Continental Crust) are from Condie (1993).

897 Figure 8. Plot of (A) Σ REE versus Al₂O₃, (B) Σ REE versus K₂O, (C) La_N/Yb_N
898 versus Zr, (D) Th versus Gd_N/Yb_N, (E) Gd_N/Yb_N versus P₂O₅, and (F) Th versus La.

899 Figure 9. Ternary A-CN-K (Al₂O₃-CaO+Na₂O-K₂O) diagram in molar proportions (Nesbitt
900 and Young, 1984) for the lower Francevillian Group sediments. Data for basalt,
901 andesite, TTG (tonalite-trondhjemite-granodiorite), and granite are from Condie
902 (1993). The arrows 1, 2, 3, and 4 indicate possible weathering trends for
903 unmetasomatized basalt, andesite, TTG, and granite, respectively.

904 Figure 10. Trace element discriminant plots of (A) Th/Cr versus La/Cr (after Bhatia and
905 Crook, 1986), (B) Th/Sc versus La/Sc (after Bhatia and Crook, 1986), (C) La/Th

906 versus Hf (after Floyd and Leveridge, 1987), and (D) Cr/V versus Y/Ni (after Ghosh et
 907 al., 2016) for the studied sediments. Potential sources are plotted for comparison. B:
 908 basalt; LAUCC: Late Archean Upper Continental Crust; TTG: tonalite-trondhjemite-
 909 granodiorite. Data for basalt, LAUCC, TTG, felsic volcanics, and granite are from
 910 Condie (1993).

911 Figure 11. Plots of (A) $\epsilon_{Nd(t)}$ versus Th/Sc and (B) $f^{Sm/Nd}$ versus $\epsilon_{Nd(t)}$ (after McLennan et al.,
 912 1993), excluding altered samples, BA 11_13.9 and GR_243.1, with anomalous $\epsilon_{Nd(t)}$
 913 values. Data for the Late Archean Upper Continental Crust (LAUCC), MORB, and
 914 Arc Andesite are from Taylor and McLennan (1985), and Sm-Nd isotopic data for the
 915 Gabon basement rocks (pink granite and grey TTG) are from Thiéblemont et al.
 916 (2009).

917 Figure 12. Trace elements tectonic discriminant plots for the studied sediments (after Bhatia
 918 and Crook, 1986): (A) La-Th-Sc ternary diagram, (B) Th-Sc-Zr/10 ternary diagram,
 919 (C) La/Y versus Sc/Cr diagram, and (D) Ti/Zr versus La/Sc diagram. PM: Passive
 920 Margin, ACM: Active Continental Margin, CIA: Continental Island Arc, and OIA:
 921 Oceanic Island Arc.

922

923 List of tables

924 Table 1. Sm-Nd whole-rock isotope data for the FB₁ Member and FA Formation sediments.
 925 Sm-Nd isotopic data for Gabon basement rocks (pink granite and grey TTG) are from
 926 Thiéblemont et al. (2009).

927 Table 2. Modelled fractions of compositionally different Archean crust in the analyzed
 928 samples.

929

930 Appendix

931 Figure A1. Major element spider diagrams of (A) FB₁ Member mudstones, (B) FA Formation
932 mudstones, and (C) FA Formation sandstones, normalized to the composition of the
933 Late Archean Upper Continental Crust (LAUCC; from Condie, 1993).

934 Figure A2. Plot of Sm/Nd ratios versus $^{143}\text{Nd}/^{144}\text{Nd}_{(2.1 \text{ Ga})}$. Sm-Nd isotopic data for Gabon
935 basement rocks (pink granite and grey TTG) are from Thiéblemont et al. (2009).

936 Table A1. Whole-rock major element geochemical data for the studied sediments. CIA
937 (Chemical Index of Alteration) = $(\text{Al}_2\text{O}_3/(\text{Al}_2\text{O}_3 + \text{CaO}^* + \text{Na}_2\text{O} + \text{K}_2\text{O})) \times 100$, where
938 CaO* correspond to CaO content corrected for CaO concentrations in carbonate and
939 apatite.

940 Table A2. Whole-rock trace element geochemical data for the studied sediments.

941 Table A3. Whole-rock Rare Earth Element geochemical data for the studied sediments. Eu
942 anomaly, $\text{Eu}/\text{Eu}^* = \text{Eu}_N/(\text{Sm}_N \cdot \text{Gd}_N)^{0.5}$ (Taylor and McLennan, 1985). N refers to the
943 chondrite-normalized value.

944 Conceived and designed research: Olabode M. Bankole, Abderrazak El Albani and Andrey
945 Bekker; Analyzed data: Olabode M. Bankole and Marc Poujol; Interpret data, wrote, and
946 review paper: Olabode M. Bankole, Abderrazak El Albani, Alain Meunier, Marc Poujol, and
947 Andrey Bekker

948

949

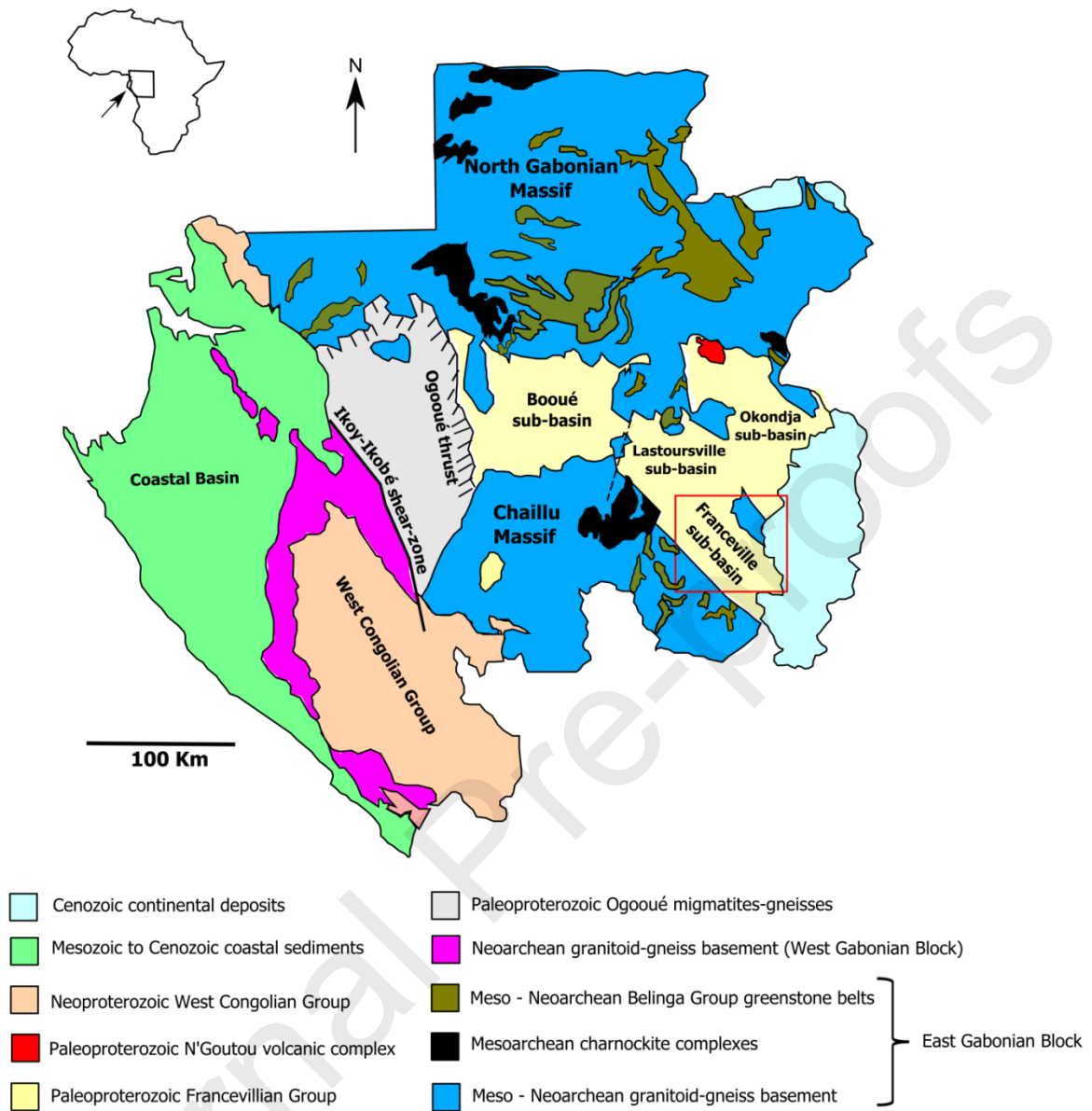


Figure 1

950

951

952

953

954

955

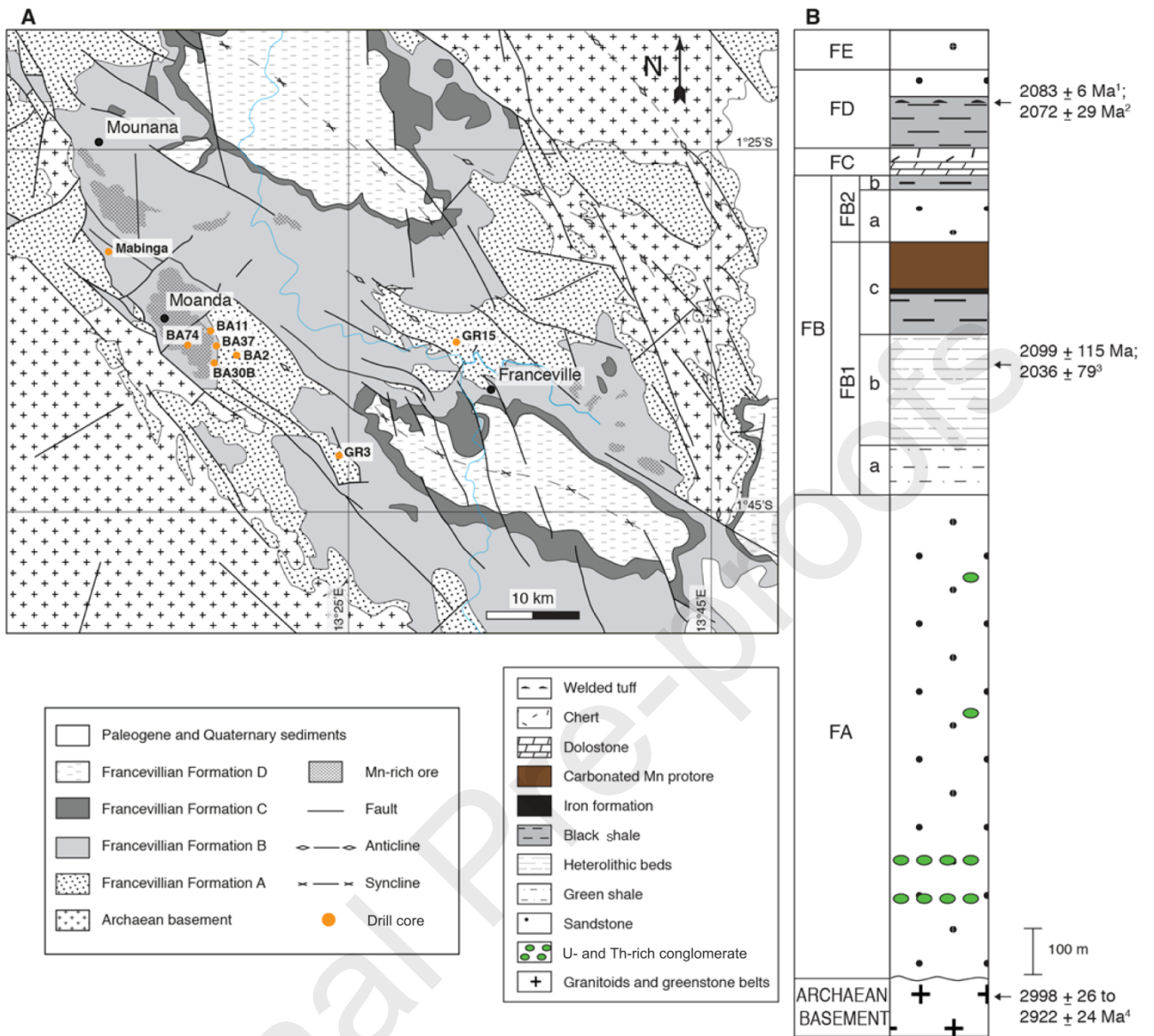


Figure 2

956
957
958
959
960
961
962
963
964
965

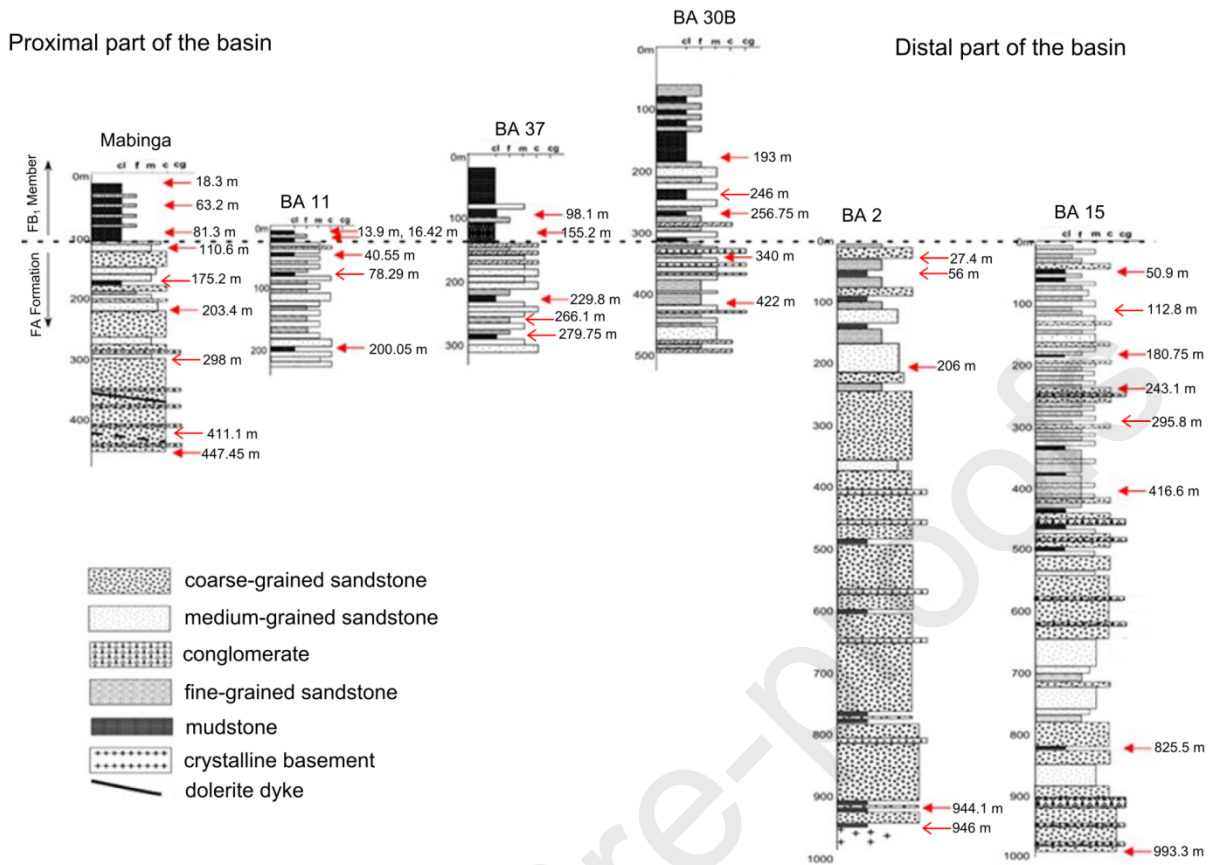


Figure 3

966
 967
 968
 969
 970
 971
 972
 973
 974
 975
 976
 977
 978
 979

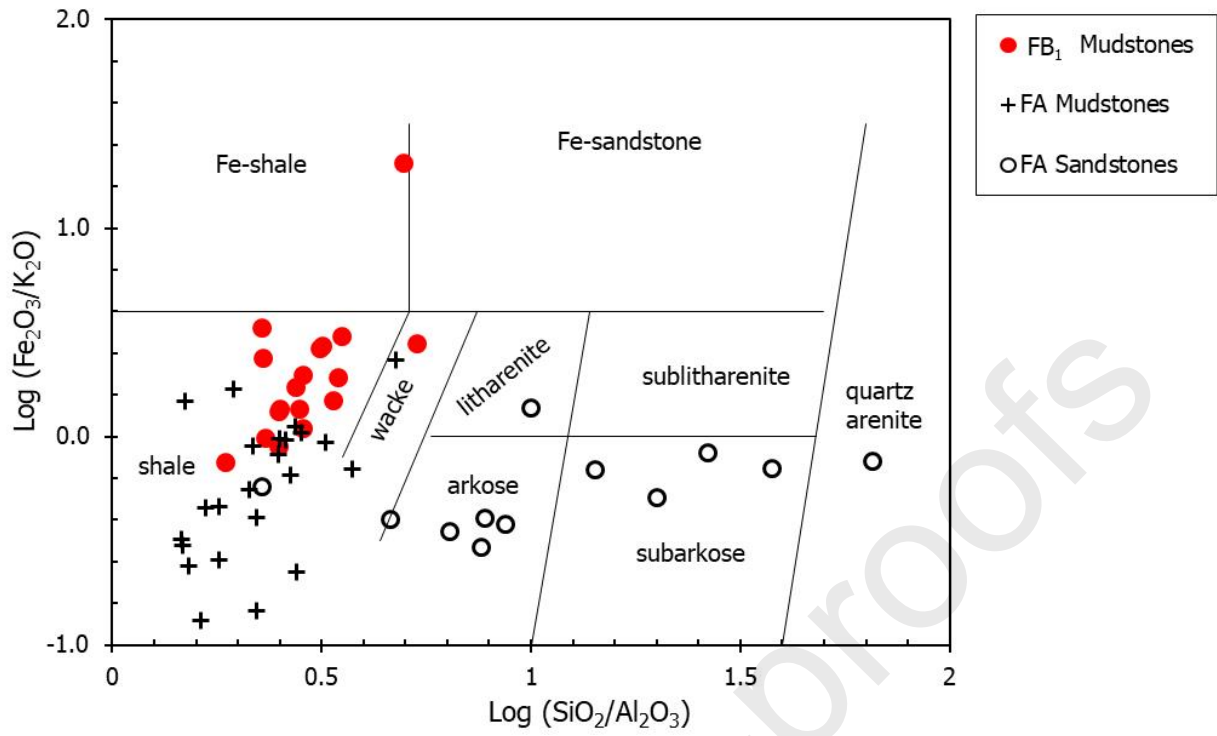


Figure 4

980

981

982

983

984

985

986

987

988

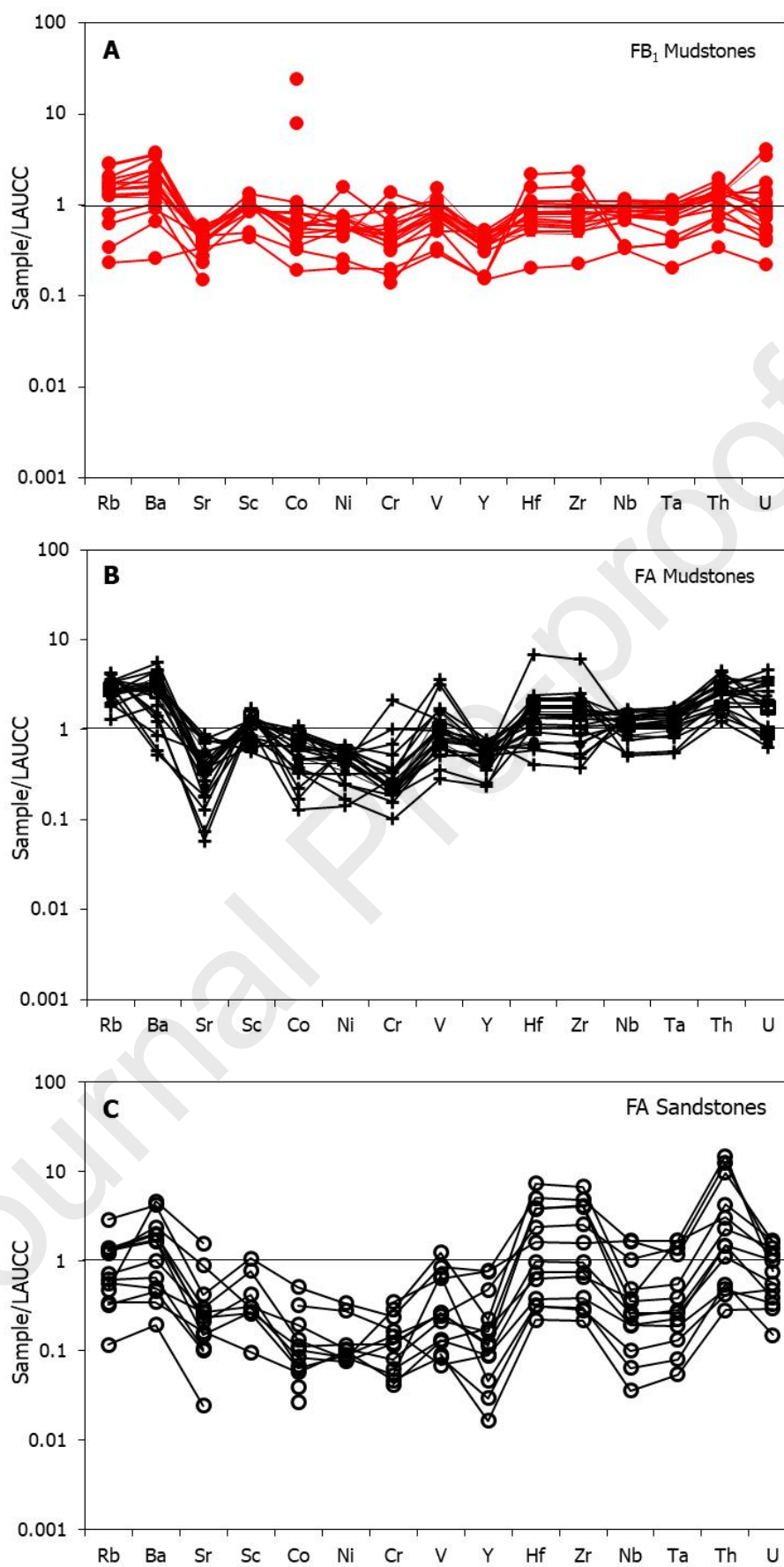
989

990

991

992

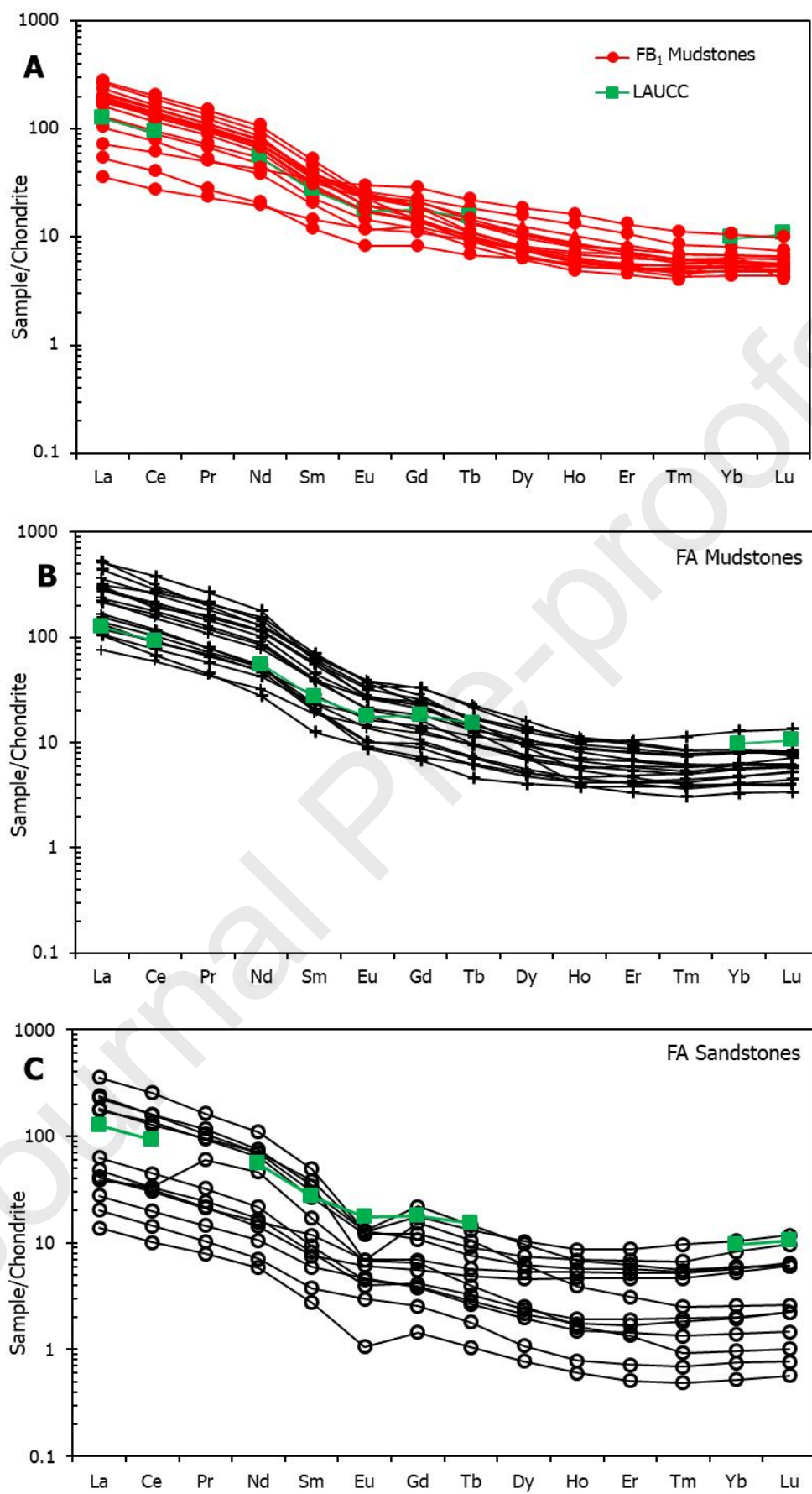
993



994

995

Figure 5



996

997

Figure 6

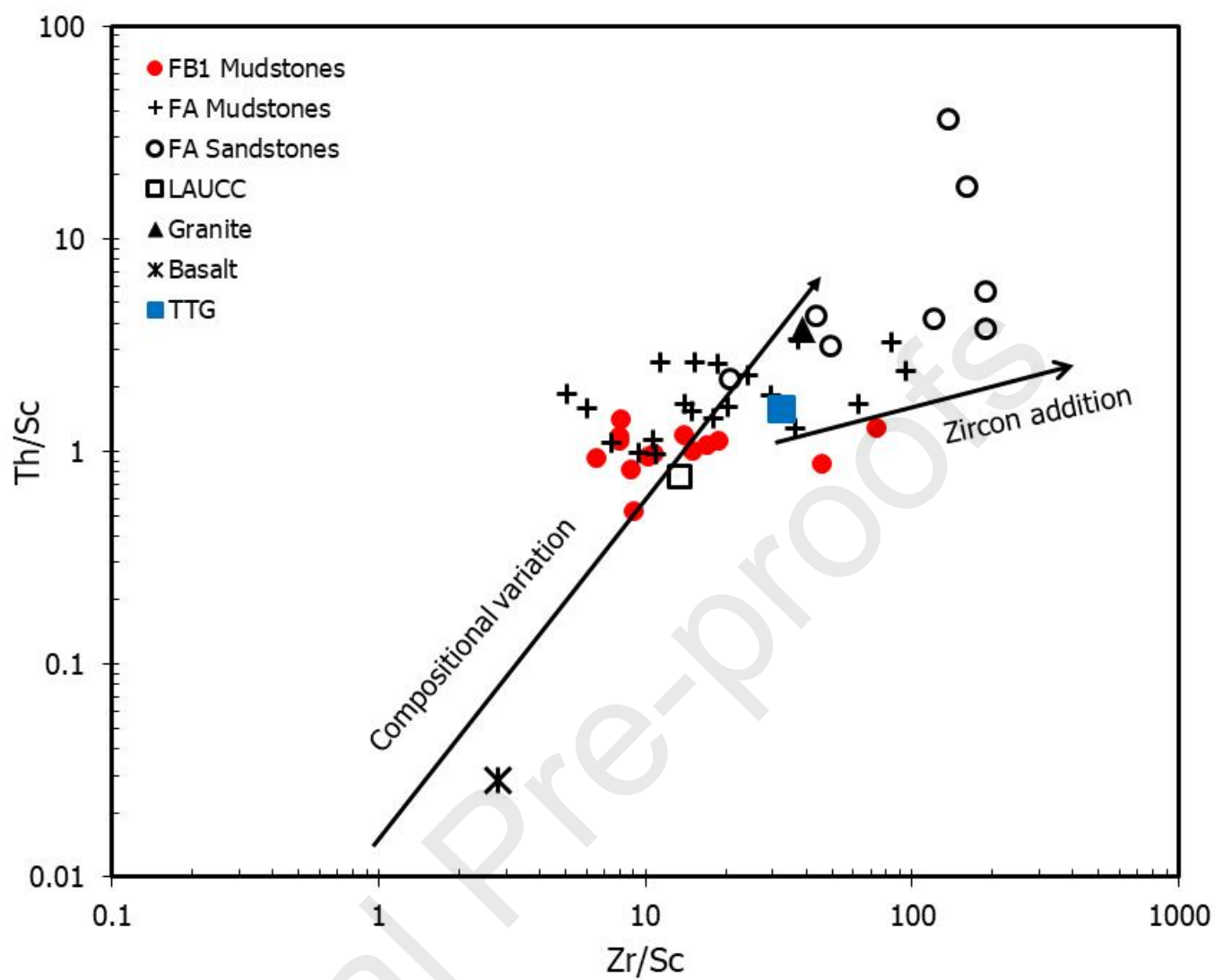


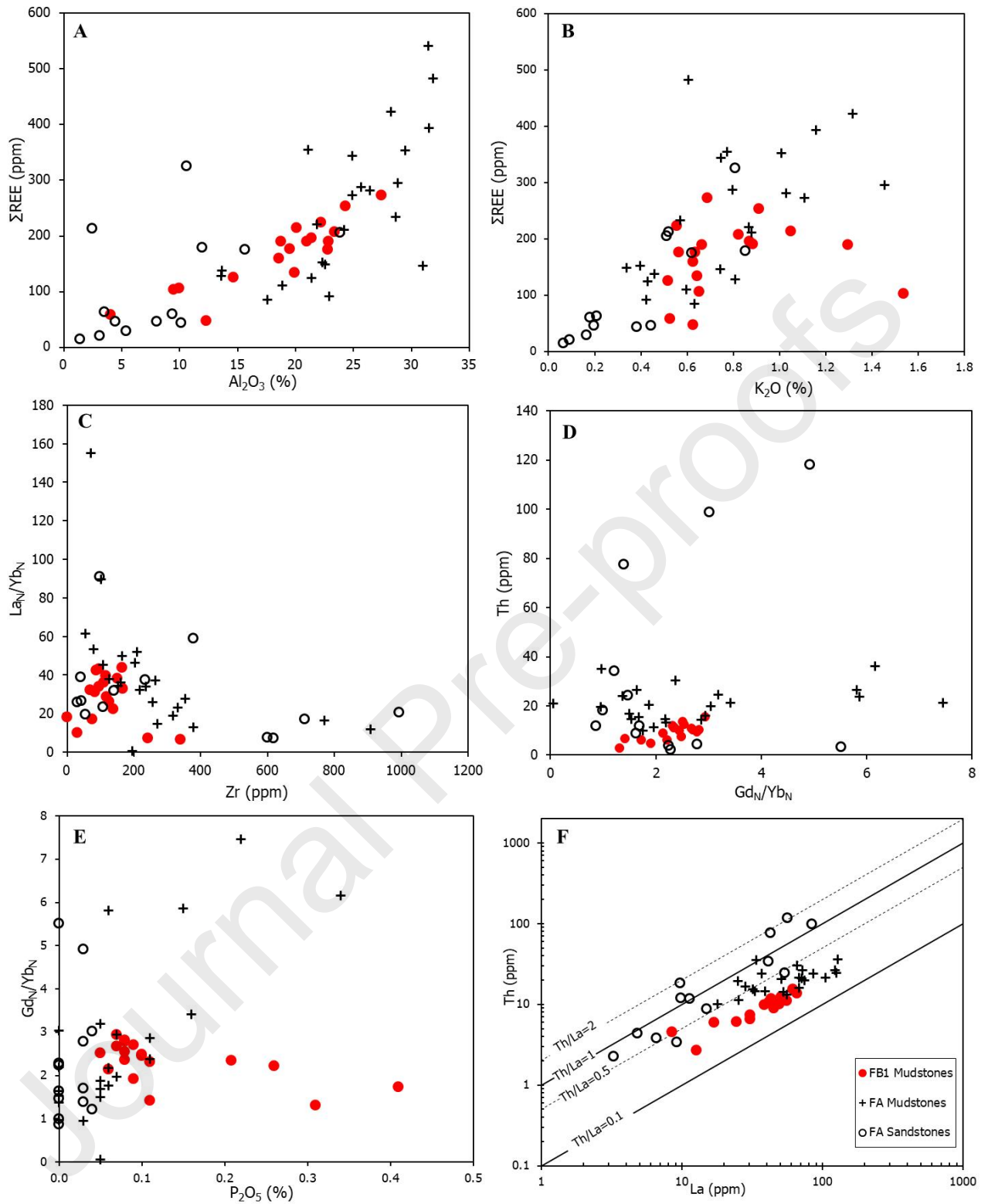
Figure 7

998

999

1000

1001



1002

1003

Figure 8

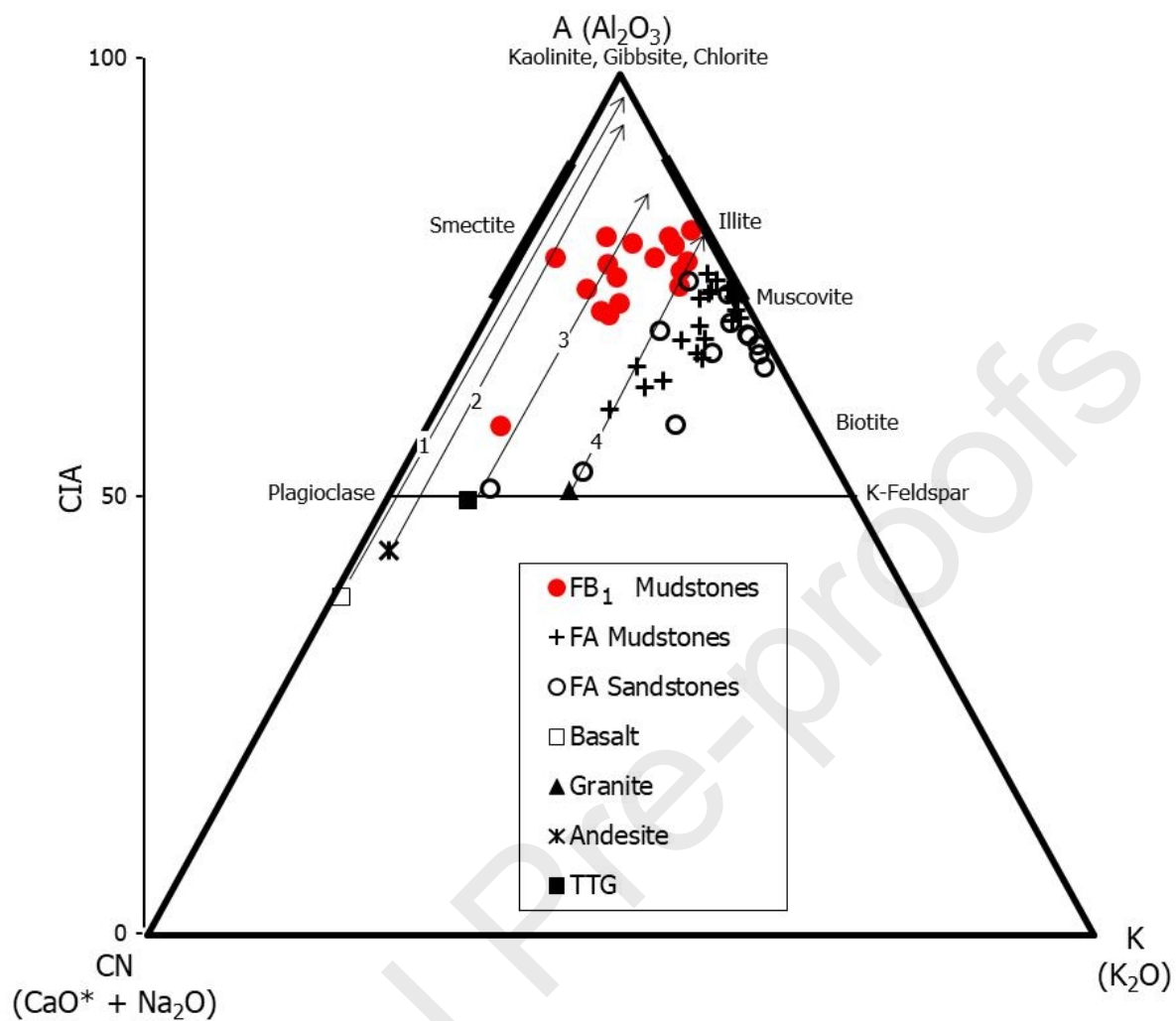


Figure 9

1004

1005

1006

1007

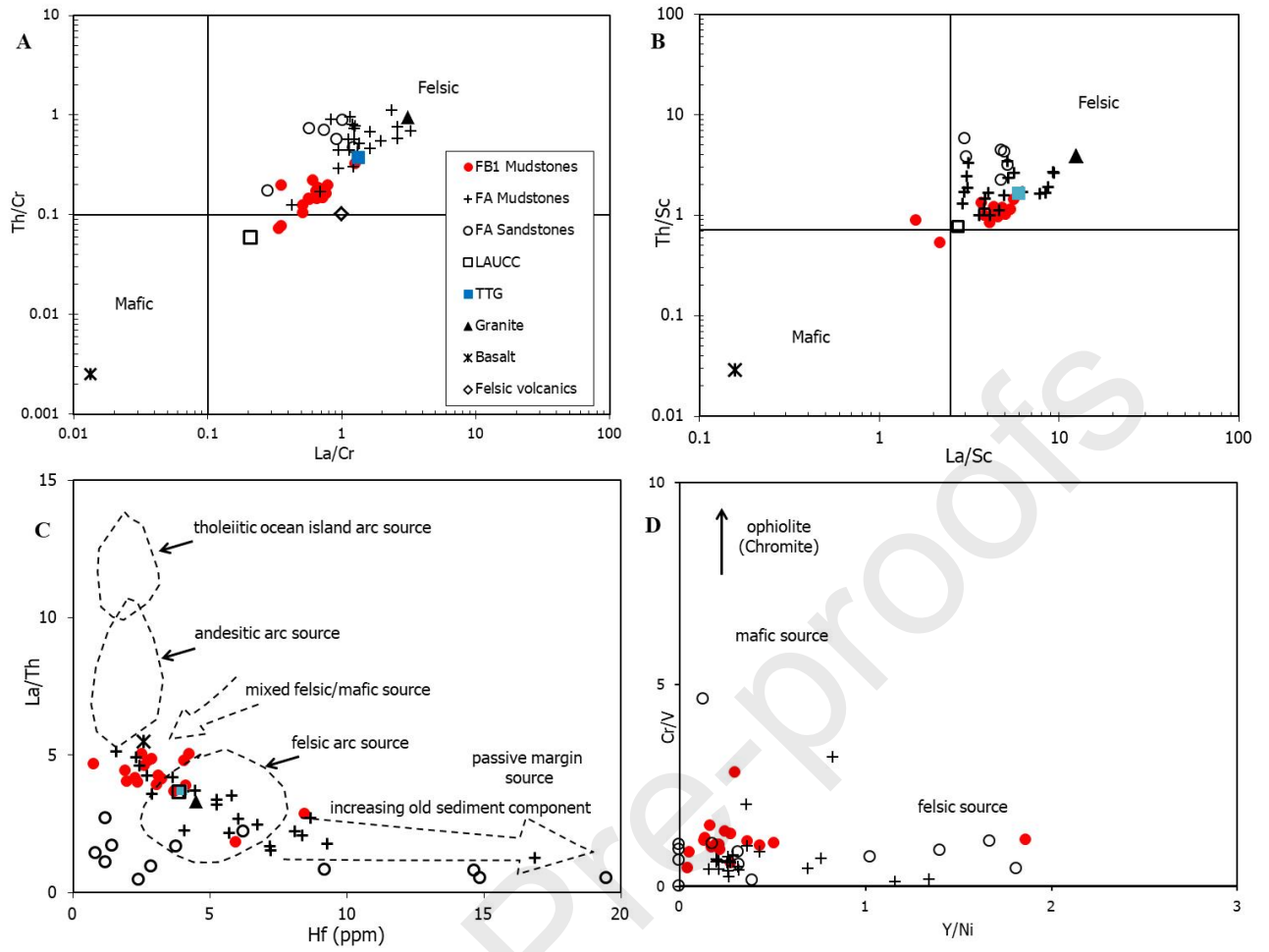
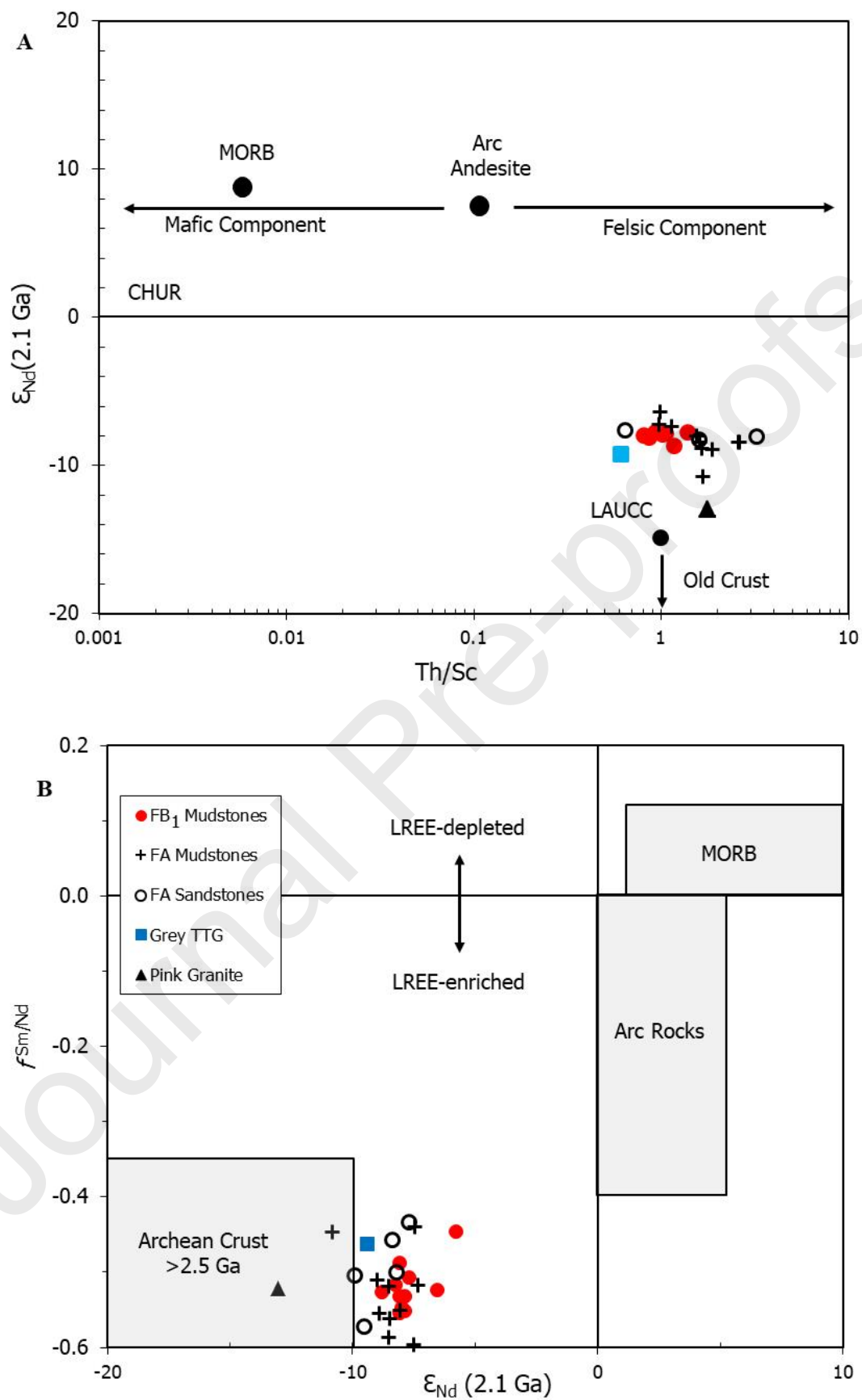


Figure 10

1008
 1009
 1010
 1011
 1012
 1013
 1014
 1015
 1016
 1017



1018

1019

Figure 11

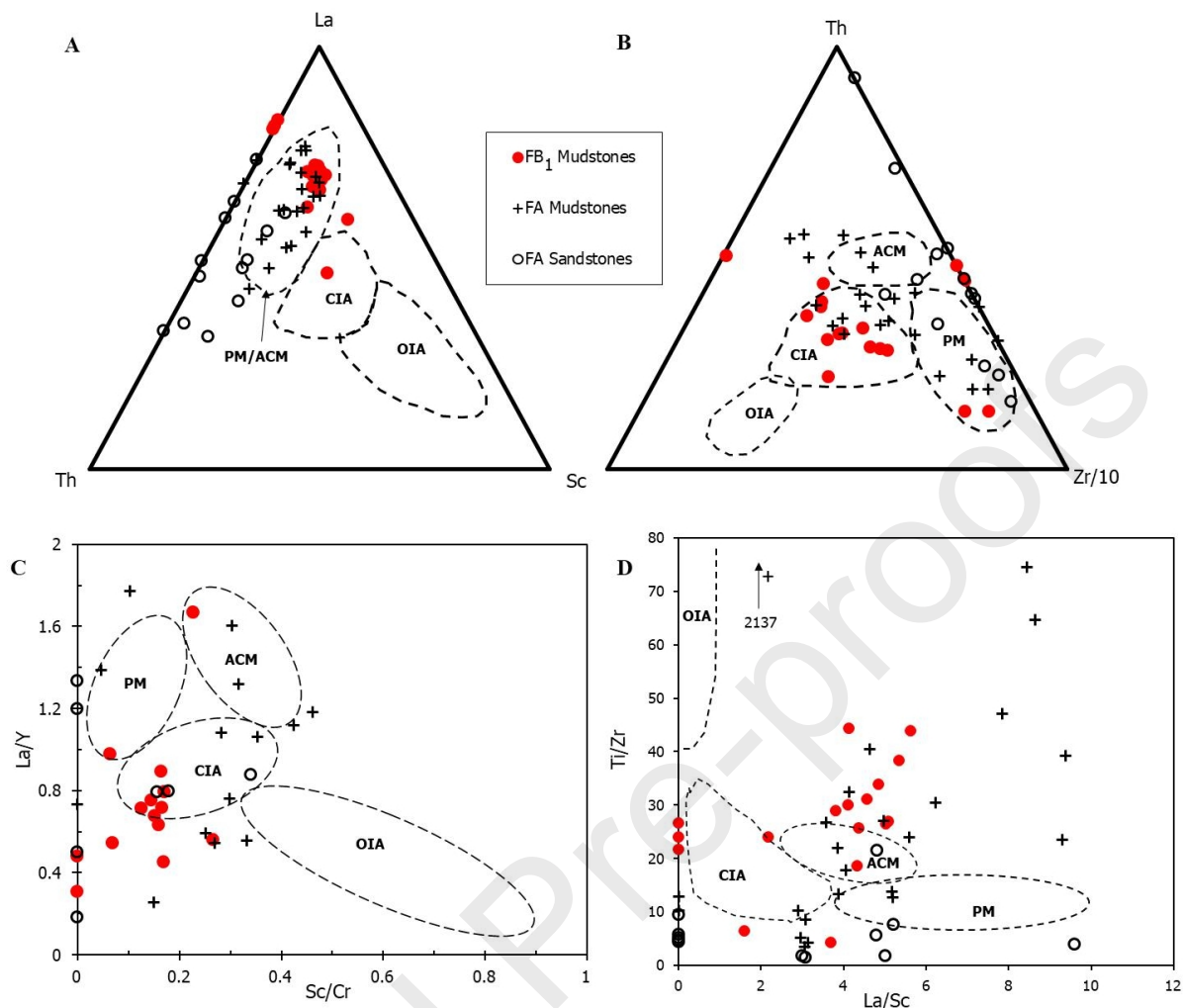


Figure 12

1020

1021

1022

1023

1024

1025

1026

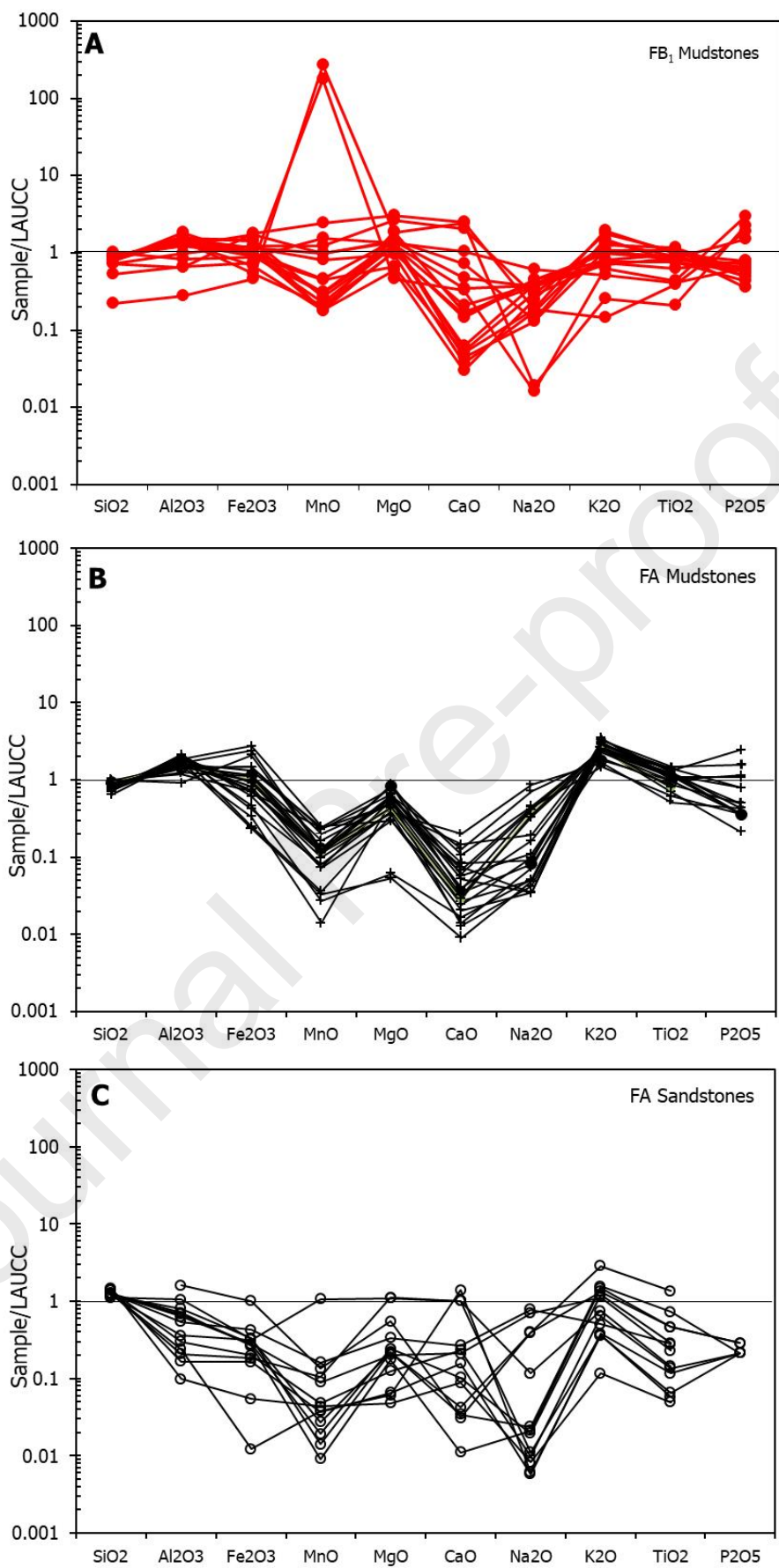


Figure A1

1027

1028

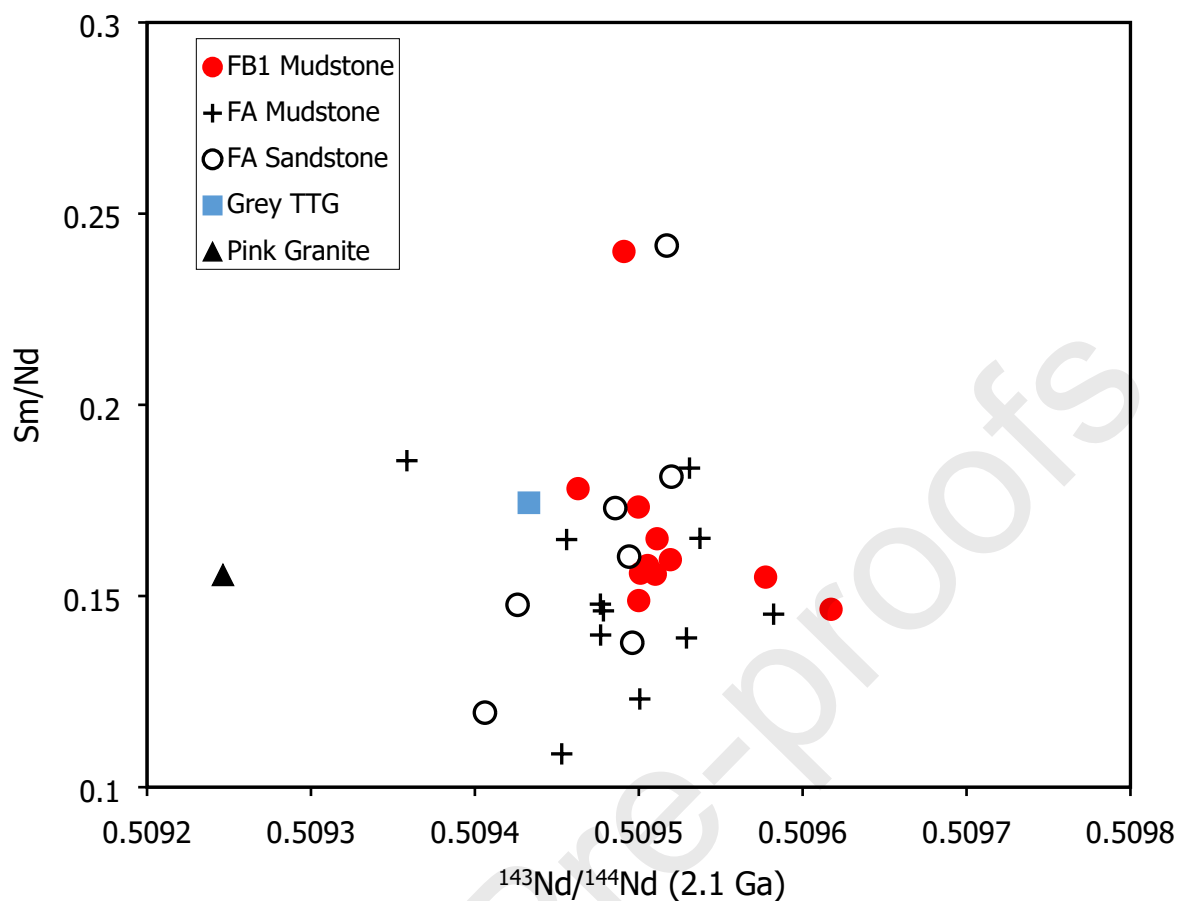


Figure A2

1029

1030

1031

1032

1033 Highlights

- 1034 • Sediments have undergone moderate weathering and secondary alteration
- 1035 • Sediments mainly derived from felsic source with minor mafic components
- 1036 • Provenance from Mesoproterozoic East Gabonian block with no juvenile contribution
- 1037 • Sediments sourced from crustal addition and recycling of differentiated granitoids

1038

1039

1040 Declaration of interests

1041

- 1042 The authors declare that they have no known competing financial interests or personal
1043 relationships that could have appeared to influence the work reported in this paper.

1044

1045

1046

1047

1048

Journal Pre-proofs